USGS
science for a changing world

Gravity Surveys for Estimating Possible Width of Enhanced Porosity Zones Across Structures on the Coconino Plateau, Coconino County, North-Central Arizona

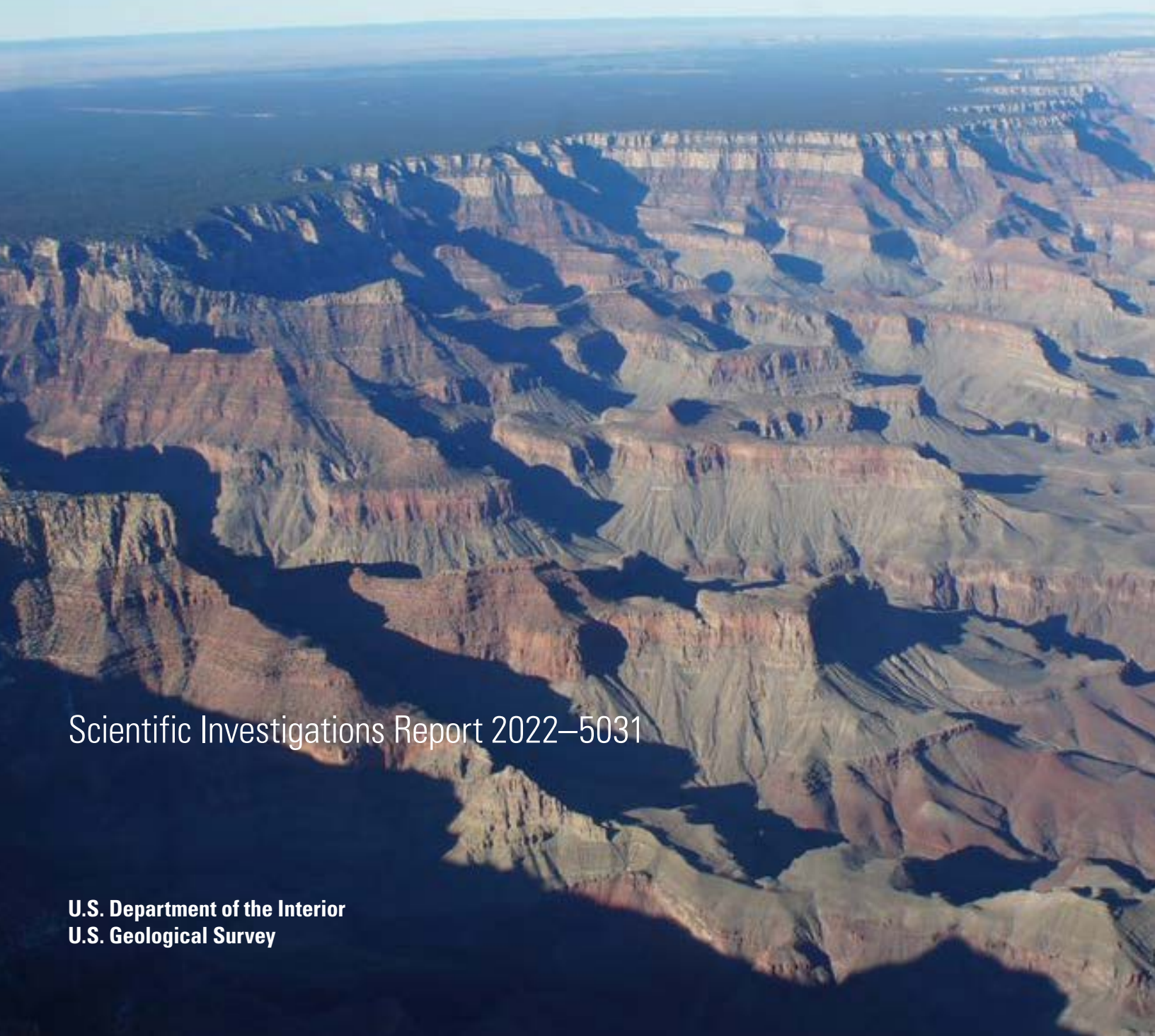

Scientific Investigations Report 2022–5031

U.S. Department of the Interior
U.S. Geological Survey

Cover. Photograph overlooking the south rim of the Grand Canyon where it coincides with the Coconino Plateau. View is from above, looking southwest. U.S. Geological Survey Photograph taken by Jon Mason on January 14th, 2012.

Gravity Surveys for Estimating Possible Width of Enhanced Porosity Zones Across Structures on the Coconino Plateau, Coconino County, North-Central Arizona

By Libby M. Wildermuth

Scientific Investigations Report 2022–5031

U.S. Department of the Interior
U.S. Geological Survey

U.S. Geological Survey, Reston, Virginia: 2022

For more information on the USGS—the Federal source for science about the Earth, its natural and living resources, natural hazards, and the environment—visit https://www.usgs.gov or call 1–888–ASK–USGS.

For an overview of USGS information products, including maps, imagery, and publications, visit https://store.usgs.gov.

Suggested citation:
Wildermuth, L.M., 2022, Gravity surveys for estimating possible width of enhanced porosity zones across structures on the Coconino Plateau, Coconino County, Arizona: U.S. Geological Survey Scientific Investigations Report 2022–5031, 22 p., https://doi.org/10.3133/sir20225031.

Associated data for this publication:
Wildermuth, L.M., 2021, Data from "Gravity surveys for estimating possible width of enhanced porosity zones across structures on the Coconino Plateau, Coconino County, north-central Arizona": U.S. Geological Survey data release, https://doi.org/10.5066/P9ZYHEBB.

ISSN 2328-0328 (online)

Contents

Figures

Tables

Conversion Factors

U.S. customary units to International System of Units

Multiply	By	To obtain
	Length	
foot (ft)	0.3048	meter (m)

International System of Units to U.S. customary units

Multiply	By	To obtain
	Length	
centimeter (cm)	0.3937	inch (in.)
meter (m)	3.281	foot (ft)
kilometer (km)	0.6214	mile (mi)
	Density	
kilogram per cubic meter (kg/m^3)	0.06242	pound per cubic foot (lb/ft^3)
	Volume	
cubic meter (m^3)	264.2	gallon (gal)
cubic meter (m^3)	35.31	cubic foot (ft^3)

Datum

Vertical coordinate information is referenced to North American Vertical Datum of 1988 (NAVD 88).

Horizontal coordinate information is referenced to the North American Datum of 1983 (NAD 83).

Abbreviations

ADWR	Arizona Department of Water Resources
DEM	Digital elevation model
GPS	Global Positioning System
GWSI	Ground-Water Site-Inventory System
NAD 83	North American Datum of 1983
NARGFM	Northern Arizona Regional Groundwater Flow Model
NAVD 88	North American Vertical Datum of 1988
NGS	National Geodetic Survey
NOAA	National Oceanic and Atmospheric Administration
USGS	U.S. Geological Survey

Gravity Surveys for Estimating Possible Width of Enhanced Porosity Zones Across Structures on the Coconino Plateau, Coconino County, North-Central Arizona

By Libby M. Wildermuth

Abstract

The U.S. Geological Survey completed gravity transects in 2015, 2018, and 2019 over four features: the Bright Angel Fault, Bright Angel Monocline, Tusayan Graben, and Redlands Ranch Fault Zone in the Coconino Plateau, Coconino County, Arizona, to determine if the existence and width of high porosity (low density) zones could be inferred from the resulting gravity contrasts, which could be used to update groundwater models of the region. Faults and other geological structures in the Coconino Plateau are commonly thought to play a role in the movement of groundwater in the area, but limited data exist to constrain their influence. Some groundwater models of the region have used zones of enhanced permeability and porosity along or near features to model their effect on groundwater flow but have not shown sensitivity to the width of the zones used. Enhanced porosity zones in the subsurface, such as those included along or near features in some groundwater models of the region, could create small mass deficiencies detectable by microgravity methods. However, 3 of the 4 gravity transects, the Bright Angel Fault, Bright Angel Monocline, and Tusayan Graben, showed no negative gravity anomaly over the features that could indicate the presence of a low-density zone. Only the Redlands Ranch Fault Zone that had nearby collapse features showed a negative gravity anomaly that was modeled as a zone of 0.017 increased porosity about 800 meters wide, corresponding to the relative dimension and enhanced porosity used in groundwater models of the area. This study was unable to verify the existence of enhanced porosity zones at the selected locations along the other features. However, faults and other features may affect groundwater flow in different ways at different locations, and this work does not preclude the existence of enhanced porosity zones at other places along these faults.

Introduction

The study area lies in the northeast part of the Coconino Plateau, a sub-province of the Colorado Plateau south of the Colorado River in Coconino County, north-central Arizona. The Coconino Plateau terminates to the north at the Grand Canyon and to the south near San Francisco Mountain (fig. 1). Two aquifers within the sedimentary strata of the Coconino Plateau contribute groundwater to seeps and springs in the Grand Canyon and groundwater to municipal supply wells: the discontinuous Coconino aquifer and the Redwall-Muav aquifer, referred to as the C and R aquifers respectively (Bills and others, 2016; fig. 2). Increasing use of groundwater on the Coconino Plateau for municipal supplies creates a need to better understand the hydrological role of geologic structures in this area (Pool and others, 2011).

The accepted conceptual model for groundwater flow on the Coconino Plateau is that deformation associated with faults and other structures may strongly influence vertical and horizontal groundwater flow and possibly recharge distributions (Hart and others, 2002; Billingsley and others, 2006; Bills and others, 2016). Faults can affect groundwater flow in three ways: acting as conduits, across-fault barriers, or conduit-barriers, but each mechanism may control groundwater in different ways at different locations (McCallum, 2018). Typically, faults are characterized by combining geological information with hydrological data, such as water levels on either side of a fault. However, hydrological data that could be useful for fault characterization on the Coconino Plateau are almost entirely nonexistent.

Two groundwater models of the Coconino Plateau (Montgomery, 1999; Kessler, 2002) use zones of enhanced permeability and porosity near or along major structures, which create preferential pathways for groundwater flow along those features. These models limit the width of the zones of enhanced permeability and porosity to the grid size of the models. This model discretization defines a broad damage zone that is not supported by standard structural models of fracture density as a function of distance from the fault, specifically for faults with small offsets such as those in the study area. However, Kessler (2002) found that decreasing the model grid size to 500 meters (m) from the relatively larger grid size used in the Montgomery model (1999), generally did not change the model results. A third model, the Northern Arizona Regional Groundwater Flow Model (NARGFM) (Pool and others, 2011), was able to simulate observations reasonably well without explicitly modeling features as zones of enhanced permeability and porosity. None of the models simulated conduit flow in the R aquifer. Solder and others (2020) calculated groundwater velocities across the Coconino Plateau by dividing the distance between springs in the Grand Canyon and their conceptual

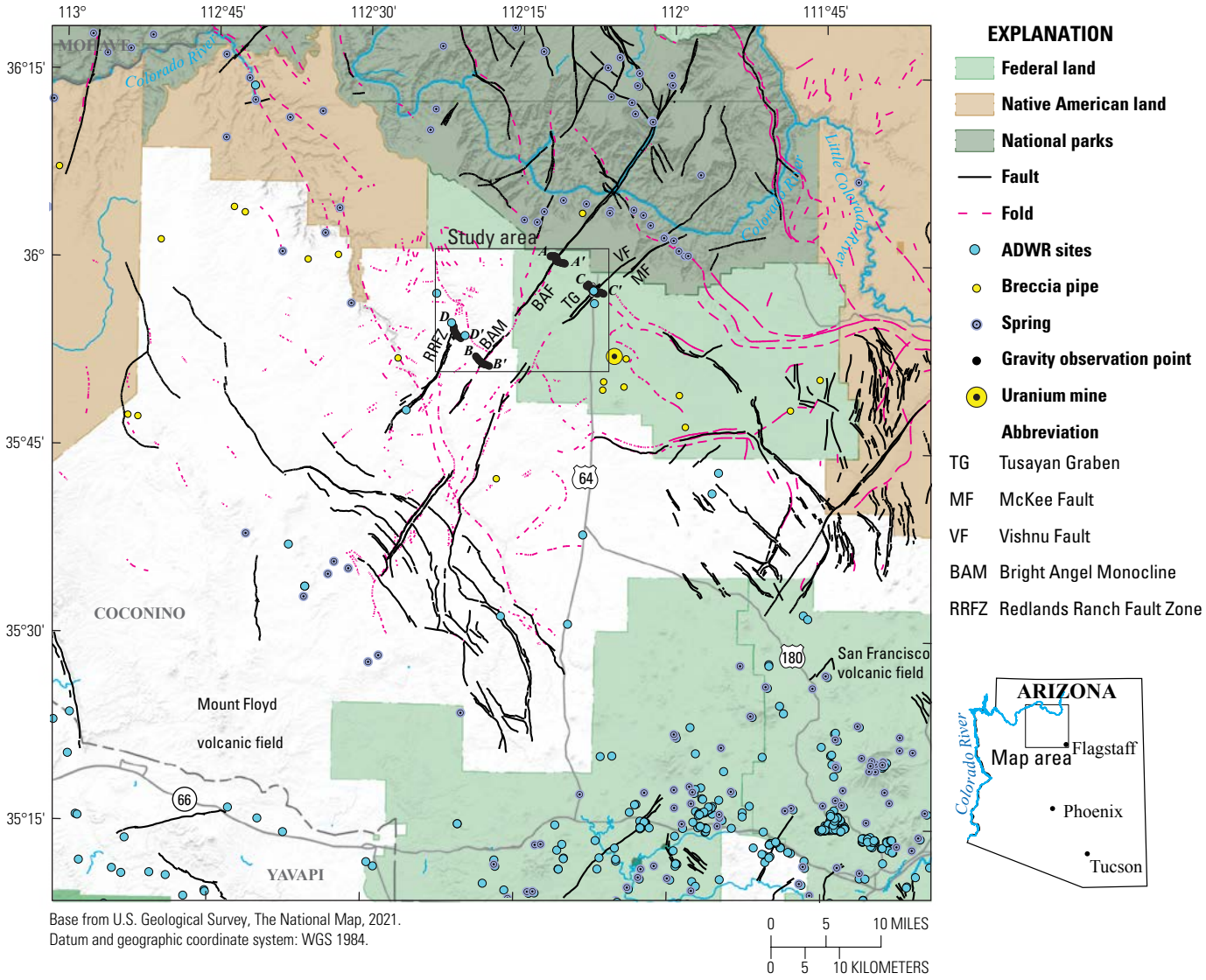

Figure 1. Map of the Coconino Plateau, Coconino County, Arizona, showing the study area, major structures, and gravity transect locations (gravity observation points) near the Grand Canyon. Structural features from Billingsley (2000) and Billingsley and others (2006). The blue dots are locations that are part of the Groundwater Site Inventory System (GWSI), of the Arizona Department of Water Resources (ADWR, 2020).

recharge source on San Francisco Mountain by mean ages in the springs and found that those velocities were consistent with expected velocities in a general karst aquifer with potential for open conduit flow (such as the R aquifer), without the addition of faults. This apparent lack of sensitivity to how or whether features are modeled as zones of enhanced permeability and porosity is likely owing to the scarcity of observation data across much of the Coconino Plateau.

For this investigation, the U.S. Geological Survey (USGS) attempted to identify the existence of zones of enhanced porosity near and across four geologic structures on the Coconino Plateau. To meet this goal, relative gravity data along four gravity transects were collected in September 2015 (Tusayan Graben), 2018 (Bright Angel Fault), and 2019 (Bright Angel Monocline and Redlands Ranch Fault Zone). Gravity transects were designed to extend across features roughly normally, and approximately 1 kilometer (km) on either side of the mapped fault or monocline axis.

Purpose and Scope

The purpose of this report is to attempt to identify the existence of zones of enhanced porosity near and across four geologic structures on the Coconino Plateau. Gravity transects were used to infer enhanced porosity, calculated as a percentage increase of the average background density of the Paleozoic strata (2,520 kilograms per cubic meter [kg/m^3], Lockrem and Best, 1983), and fracture-zone widths along the gravity transects. For example, a 5 percent increase in porosity (0.05 enhanced porosity) for a unit with a density of 2,520 kg/m^3

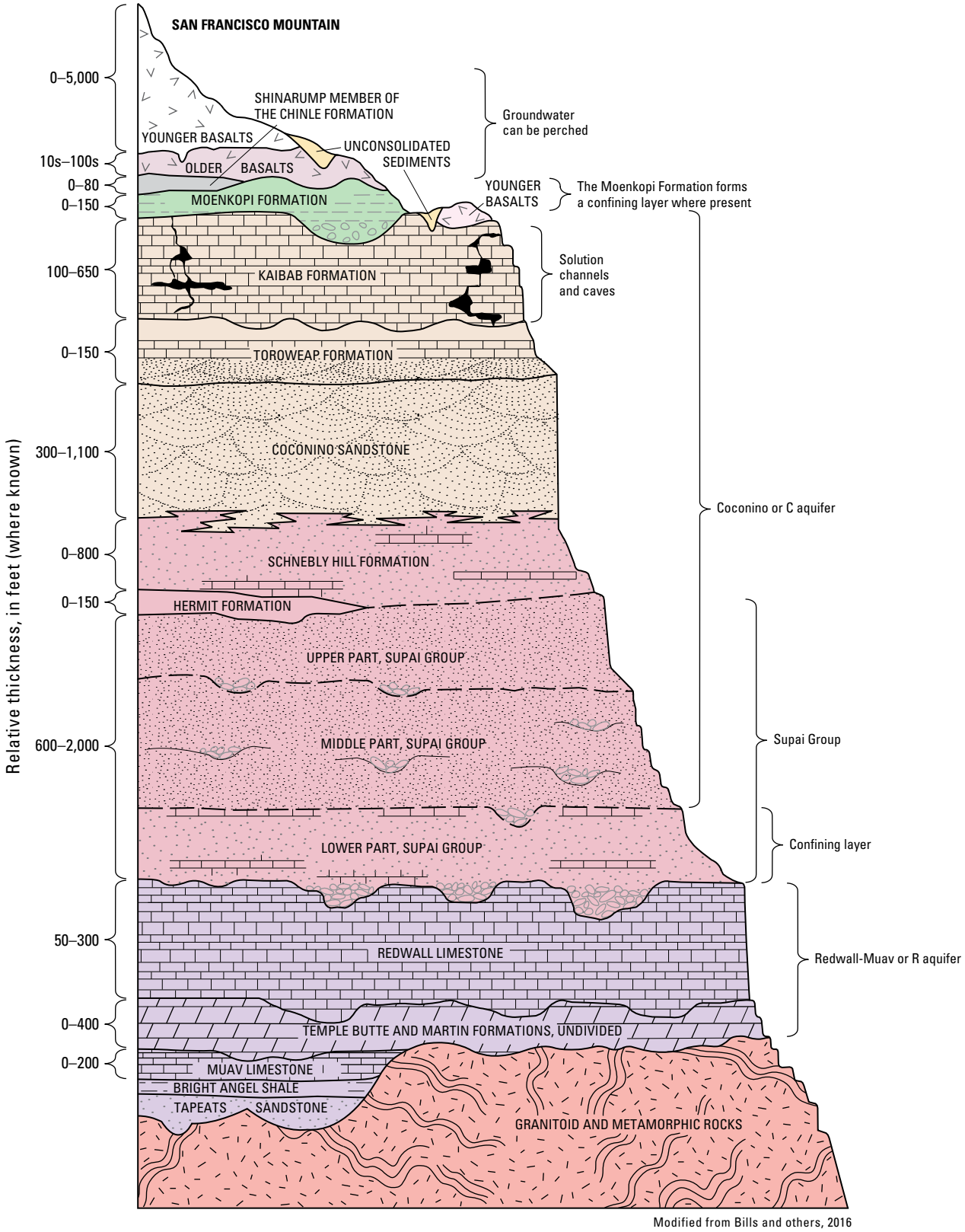

Figure 2. General stratigraphic section of rock units in the Coconino Plateau, Coconino County, Arizona. Two aquifers within the sedimentary strata of the Coconino Plateau contribute groundwater to seeps and springs in the Grand Canyon and groundwater to municipal supply wells: the discontinuous Coconino aquifer and the Redwall-Muav aquifer, referred to as the C and R aquifers, respectively.

would result in a density decrease of 126 kg/m³ (density contrast of –126 kg/m³) since the density of the additional void space is zero. Information about fracture-zone width and relative porosity may be useful to update conceptual models and groundwater-flow models for the area. The features chosen for this study are the Bright Angel Fault, Bright Angel Monocline, Tusayan Graben, and the Redlands Ranch Fault Zone (fig. 3).

Previous Investigations

The geology of different parts of the study area was investigated in some detail through the middle of the 20th century beginning with investigations of Dutton (1882) and Darton (1910) who focused on the geology and structure of northern Arizona in their reconnaissance studies of the region.

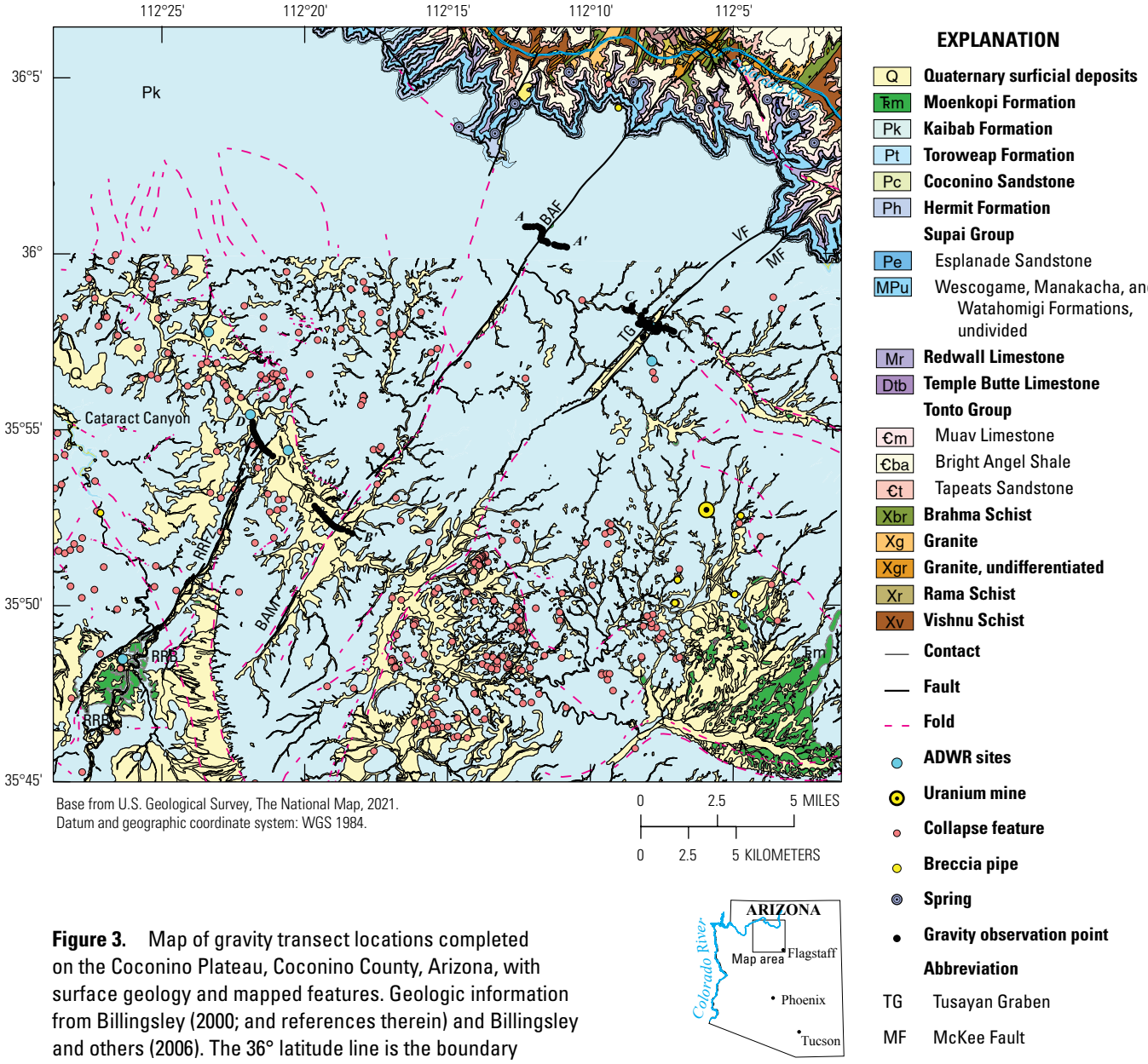

Figure 3. Map of gravity transect locations completed on the Coconino Plateau, Coconino County, Arizona, with surface geology and mapped features. Geologic information from Billingsley (2000; and references therein) and Billingsley and others (2006). The 36° latitude line is the boundary between those two studies. The blue dots are locations that are part of the Groundwater Site Inventory System (GWSI), of the Arizona Department of Water Resources (ADWR, 2020).

The geology of the Grand Canyon has been investigated by many natural and physical scientists. The Grand Canyon Natural History Association has compiled these investigations into a bibliography of the Grand Canyon and lower Colorado River as a ready reference to Grand Canyon geology (Spamer, 1990). Bills and Flynn (2002) compiled geology, hydrology, climate, and other water-resources data and reports.

The prevailing conceptual model among geologists and hydrologists is that faults on the Coconino Plateau control groundwater flow (Metzger, 1961; Huntoon, 1977; Montgomery and others, 1999; Kessler, 2002; Bills and others, 2016; Pool and others, 2011). Such features may result in vertical connectivity between the C and R aquifers where water is present in the Coconino (Huntoon, 1977; Bills and others, 2016; Billingsley and others, 2006). Huntoon (1977) also noted that faults in the region may act as both preferential pathways (conduits) and barriers.

Inkenbrandt and others (2013) used empirical methods developed by Hurlow (1998), Dutson (2005), and Savage and Brodsky (2011) to estimate the fracture density distribution and hydraulic conductivity adjacent to the Hurricane Fault in southwest Utah. Inkenbrandt and others (2013) found that hydraulic conductivity within 10 m of the fault was 15 times higher than matrix values but decreased to 2 times matrix values at about 600 m from the fault core. Savage and Brodsky (2011) also found that single faults with displacement less than 150 m (such as those in the study area) had fracture densities that decayed more rapidly with distance than faults with larger offset or multiple fractures.

Groundwater flow models of the Coconino Plateau groundwater system include Montgomery and Associates (1999), Kessler (2002), and NARGFM (Pool and others, 2011). The extents of the first two models were limited to the Coconino Plateau and were intended to model the effects of pumping resulting from planned development. NARGFM simulates groundwater flow across northern Arizona and only models the R aquifer in the Coconino Plateau area. NARGFM does not include zones of enhanced permeability along faults, but still results in a reasonably good match to existing water-level and spring discharge observations. Very little data are present that could be used to confirm the conceptual modeling of faults as zones of enhanced permeability and porosity on the Coconino Plateau. Hydrologic studies of water elevations or pumping tests near faults or folds have not been done in the study area, and few wells are available for passive monitoring (fig. 1). A study of well yields outside the study area has shown that wells completed in or near faults have higher yields than those that are not (Bills and others, 2000).

The gravitational potential of masses with various shapes stems from Newton's law and has been thoroughly developed since (for example, Blakeley, chap. 2, 1995). This work can be used to create models of the gravitational signatures of a variety of geologic features, such as those modeled by Prieto (1996), to aid identification of common features encountered during mineral exploration. The National Geodetic Survey (NGS) collected and compiled gravity observations throughout the state of Arizona (Dater and others, 1999), which have been used to create gravity anomaly maps such as the Arizona isostatic gravity anomaly map created by Sweeney and Hill (2001). Gettings and Bultman (2005) combined multiple types of regional geophysical data, including gravity, to identify major geological structures that may have hydrologic significance on the Coconino Plateau. Many studies designed to delineate fault structures will use a two-dimensional grid of data observations over a larger area, which allows for additional data processing methods. However, no such work has been done in the study area. A single transect of gravity observations collected across a fault is useful for testing a hypothesis to determine if further data collection is merited, such as was done in Phelps and others (2013) near Barstow, California, to identify and model fault offsets using only gravity data.

Setting

The study area lies in the northeast part of the Coconino Plateau, a subprovince of the Colorado Plateau south of the Colorado River in north-central Arizona (Hunt, 1967). The study area is predominantly in Coconino County, with small sections of Mohave County in the northwest corner and Yavapai County in the southwest corner. The study area just clips the southern boundary of Grand Canyon National Park, near the Grand Canyon National Park airport, and is partially within the western part of the Kaibab National Forest (fig. 1).

Climate

The climate of the Coconino Plateau is semiarid to arid, with more precipitation and colder winters at higher elevations, and less precipitation and relatively intense heat in the summer at lower elevations (Bills and others, 2016). Intense but short monsoon storms in the summer result in relatively rapid runoff, whereas milder winter storms may last longer and have lower potential evapotranspiration, which results in more potential recharge from the winter season (Bills and others, 2016).

Geology

The interior of the Coconino Plateau is a Cenozoic upland that was uplifted as part of the Colorado Plateau during the Laramide orogeny and is composed of nearly flat-lying Paleozoic and younger consolidated sediments with folds on reactivated basement faults (Huntoon, 1974; Billingsley and Hendricks, 1989; Beus and Morales, 1990). Thousands of feet of Mesozoic rocks that overlayed the Paleozoic strata were removed during the Laramide orogeny (Hunt, 1967). Cenozoic sedimentary rocks on top of Paleozoic strata were also largely eroded but may act as an upper confining unit on the C aquifer, where present (Billingsley and others, 2006; fig. 2). Erosion of sediments on the Coconino Plateau has exposed a land surface characterized by low-relief hills and mesas, broad mature valleys, and several internal drainages with no free-flowing streams. The southern third of the Coconino Plateau is covered

by Tertiary to Pleistocene volcanic rocks of the San Francisco and Mount Floyd Volcanic Fields (Billingsley and others, 2006). The hills and mesas are the scattered remnants of these rocks protected by local downwarping or lava cap rocks. The elevation of the Coconino Plateau ranges from about 1,740 ft (530 m) at the mouth of National Canyon in Grand Canyon to 12,633 ft (3,851 m) at Humphrey's Peak. Total relief for the plateau is more than 10,500 ft (3,200 m) (Bills and others, 2016). Most of the young, steep drainages are aligned on joints and faults (Billingsley, 2000; Weir and others, 1989), are small in area, and have ephemeral streamflow. These drainages can contain discharge points (such as springs) where the joints and faults in the drainage intersect the R aquifer, or the C aquifer when it is present (Bills and others, 2016).

Hydrogeology

Several stratum of the Coconino Plateau are important to groundwater flow. There are two primary aquifers: the unconfined Coconino aquifer (commonly referred to as the C aquifer), composed of the Kaibab Formation, Coconino Sandstone, and some units of the Supai Group (in places); and the confined Redwall-Muav (commonly referred to as the R aquifer) composed of the Redwall and Muav Limestone layers and the Temple Butte Formation where present (fig. 2). The deeper limestone R aquifer is thought to have dissolution features that allow unimpeded drainage and flow of groundwater through conduits (Bills and others, 2016), and the largest springs emanate from this aquifer, or at the upper confining unit of this aquifer, where it intersects the Grand Canyon.

Smaller seeps from the C aquifer are also observed in the Grand Canyon, but most discharge from the C aquifer is thought to be directed downward, along preferential flow paths provided by geological structures such as faults or collapse features that have not become cemented (Bills and others, 2016). Discharge from the C aquifer may reach the R aquifer only where that aquifer's confining layer (lower part of the Supai Group) is absent, or where faults and fractures have penetrated that unit. The C aquifer is discontinuous across the Coconino Plateau, and not well-mapped, adding to the difficulty of understanding and modeling C and R aquifer connectivity. The R aquifer is largely underlain by the impermeable Bright Angel Shale of the Tonto Group, which limits flow into less conductive Precambrian layers.

Bright Angel Fault

The Bright Angel Fault is a discontinuous fault approximately 40 km long, that extends southwest from the Grand Canyon (fig. 3). It continues northeast from the Canyon as the Eminence Fault through the Kaibab Plateau, and it is one member of a regional system of northeast trending faults reactivated in the Cenozoic era along Precambrian faults (Shoemaker and others, 1978), with an offset in the Paleozoic strata of 61 m, southeast block down (Huntoon and Sears, 1975). The fault dips from 76 to 87 degrees (°) southeast in the Paleozoic rock, compared to a shallower dip of 45 to 80° southeast through the Precambrian strata (Huntoon and Sears, 1975). Bedding on the east block of this fault may dip towards the fault trace, which suggests extensional movement accompanying the normal faulting in more recent time (Billingsley and others, 2006). The gravity transect across this feature was completed near the northern terminal of the fault, near the edge of the south rim of the Grand Canyon (fig. 4). Note that in the Grand Canyon, there are different types of bedrock on either side of the Bright Angel Fault: Brahma Schist (Ilg and others 1996; Billingsley, 2000, and references therein) to the southeast, and a mixed granite to the northwest (labeled as Xgr in Billingsley, 2000; fig. 4). Gravity contrasts across this fault may be due to both offset layers of different densities and bedrock density contrast on either side of the fault.

Approximately 19 km to the southwest, along the fault from the first gravity transect, a second transect was completed where the fault is marked as a monocline (fig. 5). A monocline is a fold, rather than a fracture, although a buried fault may exist. The Bright Angel Monocline rises sharply on the southeast side of the monocline axis, and dips to the northwest.

Redlands Ranch Fault Zone

The Redlands Ranch Fault Zone begins along the west edge of the Redlands Ranch Basin, which is a large circumference collapse feature Billingsley and others (2006) identified as the lowest structural point on the Coconino Plateau, with preserved Cenozoic strata downdropped to the southeast approximately 60 m (fig. 3). Small fault segments with unknown offset and scattered collapse features continue northeast of the basin, and the gravity transect for this location is located at the northern terminal of this fault zone. The transect crosses one segmented fault and is approached by two additional faults and a sequence of sinkholes or collapse features (fig. 5).

The geology of the basin shows preserved Moenkopi Formation (largely eroded elsewhere on the Coconino Plateau), which may act as an upper confining unit for the C aquifer, and some Quaternary alluvial fill. The area where the gravity transect crosses the Redlands Ranch Fault Zone is largely composed of Kaibab Formation overlain in places by Quaternary alluvium. There are two wells, labeled as sites 1 and 2 (see table 1 and fig. 5), near the gravity transect with water levels near 300 m below land surface recorded after initial construction in 1966 (table 1), indicating there once was some water in the discontinuous C aquifer at that depth.

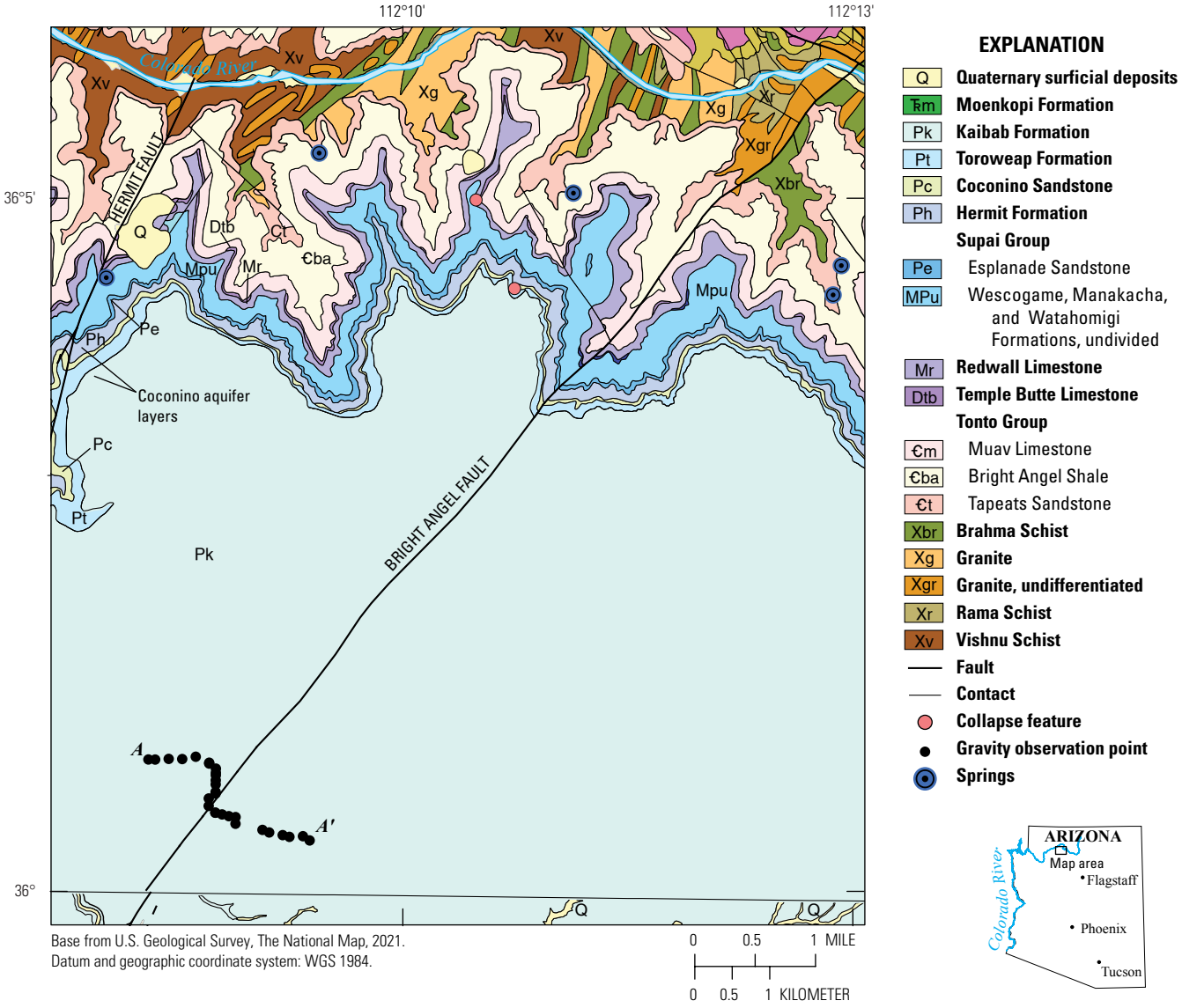

Figure 4. Closeup map of the gravity transect (gravity observation points) across the Bright Angel Fault near the Grand Canyon, in the Coconino Plateau, Coconino County, Arizona. The Redwall-Muav or R aquifer layers (Redwall Limestone, Temple Butte Formation [Fm], and Muav Fm) and Coconino or C aquifer layers (Kaibab Fm, Toroweap Fm, Coconino Sandstone, Hermit Fm, and Supai Group) are indicated. Note: the C aquifer is not continuous in the study area. Geologic information from Billingsley, 2000.

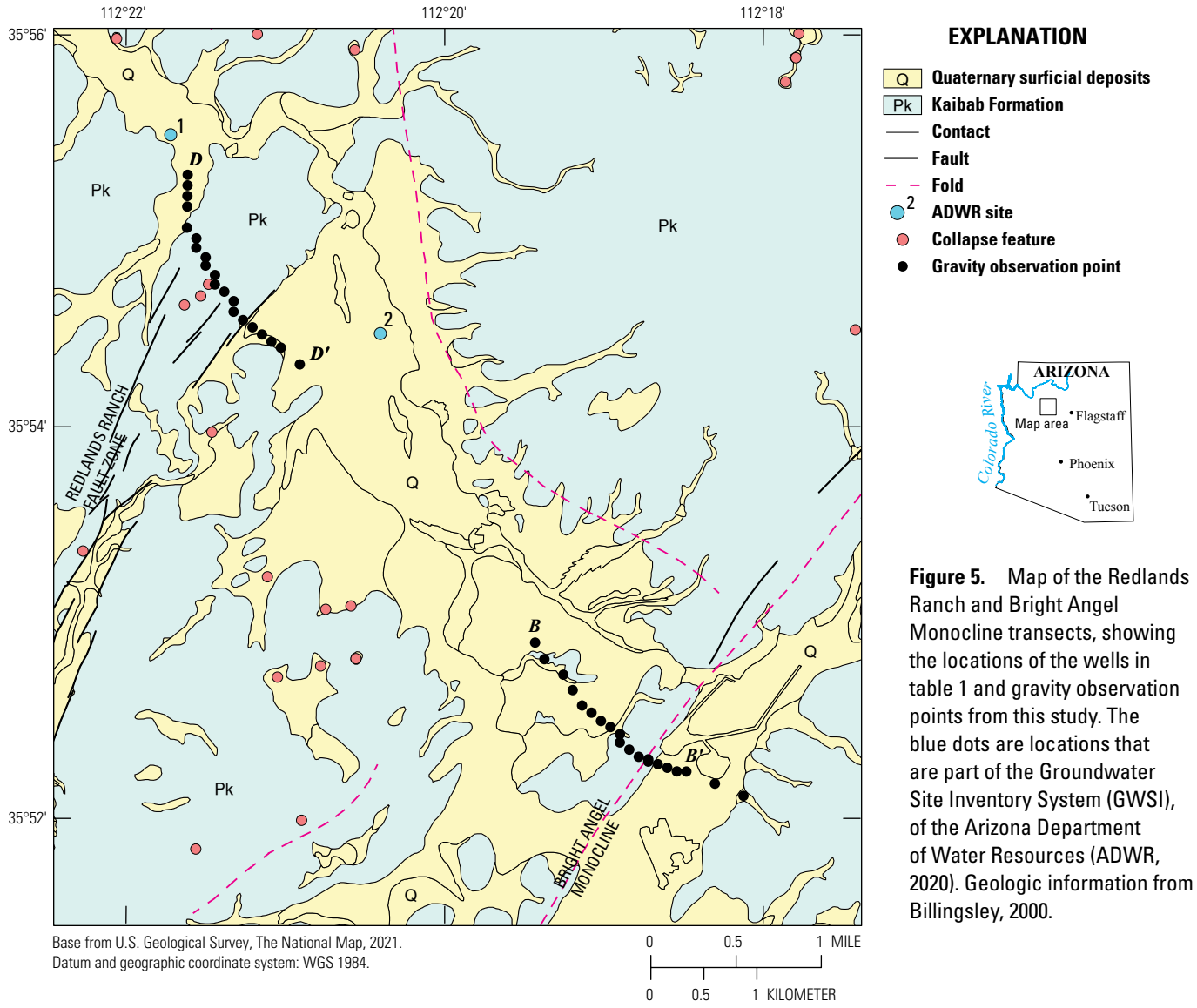

Figure 5. Map of the Redlands Ranch and Bright Angel Monocline transects, showing the locations of the wells in table 1 and gravity observation points from this study. The blue dots are locations that are part of the Groundwater Site Inventory System (GWSI), of the Arizona Department of Water Resources (ADWR, 2020). Geologic information from Billingsley, 2000.

Table 1. Water well information from the Arizona Department of Water Resources (ADWR).

[The first two wells (labeled 1 and 2) are in the Redlands Ranch transect area (fig. 5), the remaining wells (3–6) are in the Tusayan Graben area (fig. 6). m, meters; DTW blsd, depth to water below land surface datum; N/A, no information available.]

Well number	No.	Use	Depth (m)	DTW blsd (m)	DTW date
355530113214001	1	stock	323	301	7/1/1966
355430112202001	2	stock	329	292	10/1/1966
355830112081001	3	unused	223	123	7/25/2017
55-542928	4	production	914	732	N/A
355811112074501	5	production	947	N/A	N/A
55-560179	6	production	951	732	N/A

Tusayan Graben

The Tusayan Graben is a downdropped block south of the town of Tusayan, Ariz., that is up to 500 m wide and approximately 6 km long, formed between two normal faults (fig. 6). Within the graben, Kaibab Formation is downdropped, resulting in a topographic low that may accumulate unconsolidated sediments with a lower density (fig. 6). This typically results in a negative gravity anomaly over the graben that is relatively flat, with steep gradients on either side of the graben corresponding to the bounding faults. The topographic relief of the Tusayan Graben in the area of the gravity transect is only approximately 10 m.

Methods

Gravity surveys

Relative gravity data along four gravity transects were collected in September 2015 (Tusayan Graben), 2018 (Bright Angel Fault), and 2019 (Bright Angel Monocline and Redlands Ranch Fault Zone) using Zero-Length Spring, Inc., Burris relative-gravity meter B44. Gravity transects were designed to extend across features roughly normally, and approximately 1 km on either side of the mapped fault or monocline axis. All gravity transects in this study followed roads to limit instrument tares and drift caused by vibrations to

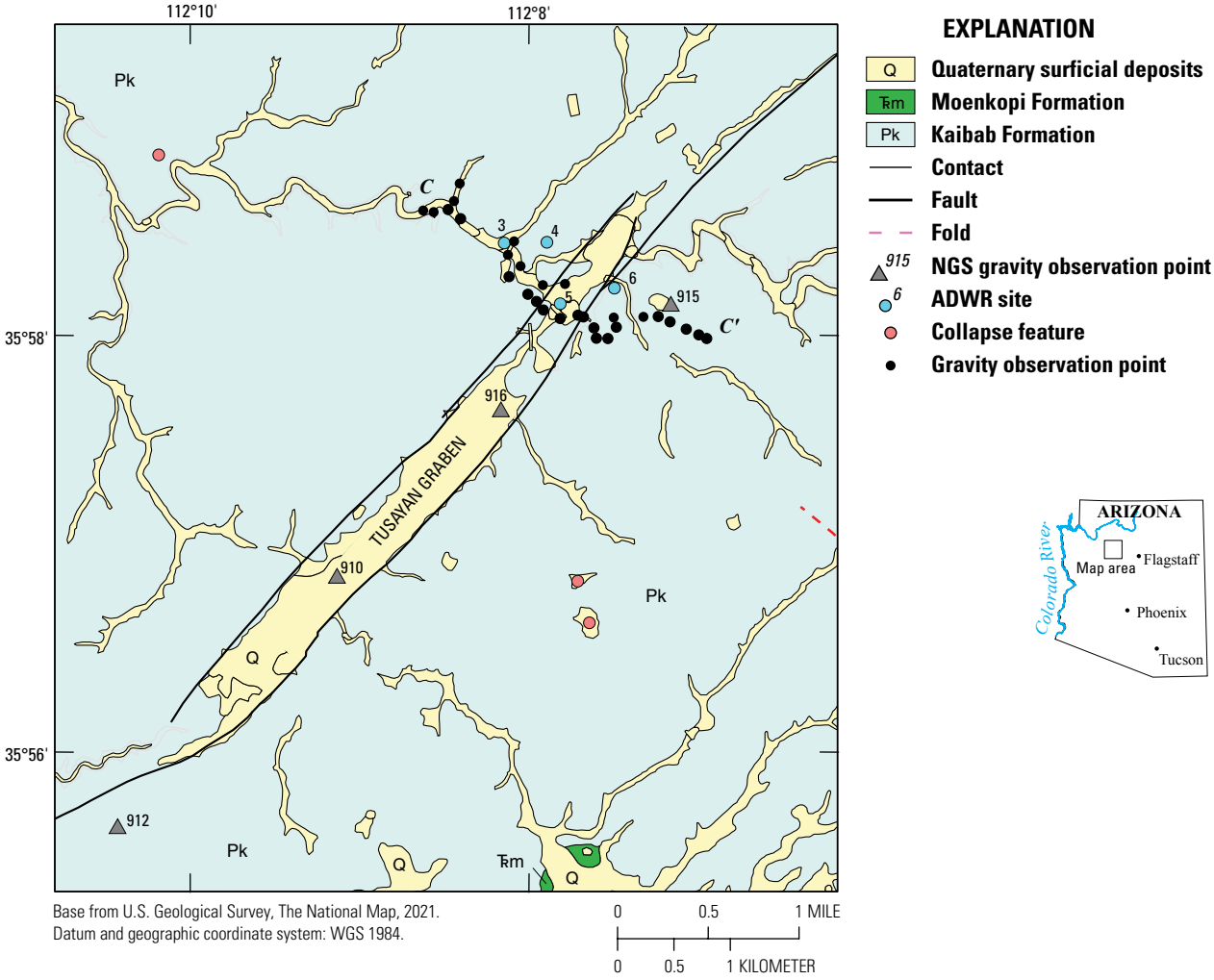

Figure 6. Map of the Tusayan Graben transect, showing the locations of the wells in table 1 and National Geodetic Survey (NGS) gravity observation points with their gravity residual values, in milligal (Dater and others, 1999). The blue dots are locations that are part of the Groundwater Site Inventory System (GWSI), of the Arizona Department of Water Resources (ADWR, 2020). Geologic information from Billingsley, 2000.

the meter. Measurements were made approximately every 100 m along a transect, using a concrete paver set on the ground (fig. 7). Repeat observations at a common base station were made throughout the day to correct for instrument drift. Data were logged using software that applied earth tide corrections based on Global Positioning System (GPS) data collected by the logging device. An absolute gravity offset value taken from NGS stations closest to each transect was applied during a least-squares network adjustment (Hwang and others, 2002) using GSadjust software (Kennedy, 2020).

GPS data were collected at every gravity observation point using a Trimble 5800 receiver with 8-minute occupations. A Trimble 5700 receiver was located at a base station near the middle of each transect for at least four hours during each survey. Base station positions were determined using the NGS Online Positioning User Service (OPUS; available at https://www.ngs.noaa.gov/OPUS/), with horizontal accuracy of about 2 centimeters (cm) and vertical accuracy of about 3 cm, equivalent to about 0.009 milligal (mGal) accuracy in gravity.

Gravity Reduction

Several factors affect the local gravity field, one of which is anomalous geology, the target of this study. In the study area other factors include the distance from the center of mass, or elevation above sea level (free air correction, g_{fa}); the effect of mass with homogeneous density between the observation point and sea level (g_{sb}); the effect of mass owing to topography (g_t); and the regional trend including isostatic compensation (g_{reg}). The gravity residual g_r (that is, the departure from the expected observation value on the reference ellipsoid, g_0) is calculated by:

$$g_r = g_{obs} - g_0 - g_{fa} - g_{sb} + g_t - g_{reg} \quad (1)$$

These reductions provide an expected value for a gravity observation if there were no subsurface density anomalies. The gravity residual reflects density variation in the upper crust (upper crust to the surface).

Reductions were completed using QCTool software (Petros Eikon, Inc., 2018), except for the regional-trend correction, which was calculated as a linear trend with distance across a transect and removed from the data. GPS data were used to calculate the theoretical gravity value (a function of latitude) and free-air correction (a function of station height above sea level). The density used for all but the terrain reductions was 2,670 kg/m^3, which is the standard, average density used for gravity reductions. Different densities were tested for the terrain corrections for the Bright Angel Fault transect since it had the steepest terrain, but different densities for that correction resulted in offset gravity residual values with no change in the magnitude of anomalies along the transect. Therefore, the density of the Kaibab Formation, 2,450 kg/m^3 (Lockrem and Best, 1983), was used for all terrain corrections.

Figure 7. Photograph of relative gravity meter (Zero-Length Spring, Inc., Burris relative-gravity meter B44) and Global Positioning System (GPS) rover setup at an observation point for the gravity transects during this study. The study area is in Coconino Plateau, Coconino County, Arizona. U.S. Geological Survey photograph taken by Libby Wildermuth in 2019.

A 1 arc-second digital elevation model (DEM), down-sampled to 1,000 m, was used for regional terrain corrections (U.S. Geological Survey, 2020). Between 2 km and 100 km, a ⅓ arc-second DEM was used for local terrain corrections to a distance of 2 km. Sampled DEMs were exported from ArcGIS Pro as .csv files and gridded within QCTool, which was also used to calculate the terrain corrections (Esri Inc., 2020).

The regional trend correction map created from the complete Bouguer anomaly (the complete Bouguer anomaly accounts for g_{fa}, g_{sb}, g_t, and g_0, reductions) and isostatic residual anomaly maps (Sweeny and Hill, 2001) was sampled to the gravity stations, but the resolution of the map resulted in the same values for several contiguous observation points. Final regional terrain correction values for each observation point were thus interpolated by fitting a linear trend to each transect. The trend that was removed was increasing to decreasing gravity residual values, from northwest to southeast. This trend is apparent in fig. 8, which shows the main northeast–southwest trending faults in the study area bounding a gravity high to the northwest that trends in the same direction (Sweeney and Hill, 2001). Removing this trend from the gravity residual presented here isolates the effect of more local geology.

Correlation between elevation and observed gravity residuals may result from an incorrect density used in the local terrain corrections or poor resolution of elevation information

in steep terrain. Where gravity residuals and terrain appeared to be correlated, a simple linear regression between the gravity residual and elevation was checked to better estimate the validity of the correction applied and the confidence in the gravity residual calculated.

Gravity Modeling

Modeling the gravity anomaly from simulated mass of known size, shape, and density is a straightforward problem referred to as the forward model. More typically, a geologic model is built and constrained by assumptions (possibly derived from a different geophysical method, or inferred from observations), and an inversion is used to arrive at the geologic model providing the best fit. Lockrem and Best (1983) list the measured densities of several stratum that can be found in the Coconino Plateau or elsewhere, and these densities were used in the forward model for those strata, and the average density given by this report was used for layers that had not been measured (2,520 kg/m^3). Other than densities for some of the strata, limited geologic information was available for this project, so forward models were manually adjusted using FastGrav version 0.9.0 (Price, 2020). FastGrav uses the Talwani method to create the modeled gravity response to mass (Talwani and Ewing, 1960). This method assumes that mass items created as flat regions extending to the right and left by user-defined distances also extend semi-infinitely into and out of the model. All geologic models presented here are nonunique and part of an infinite set of solutions, which is typical for this type of work. A lower density feature in the subsurface creates a mass deficiency that produces a local minimum in gravitational attraction over

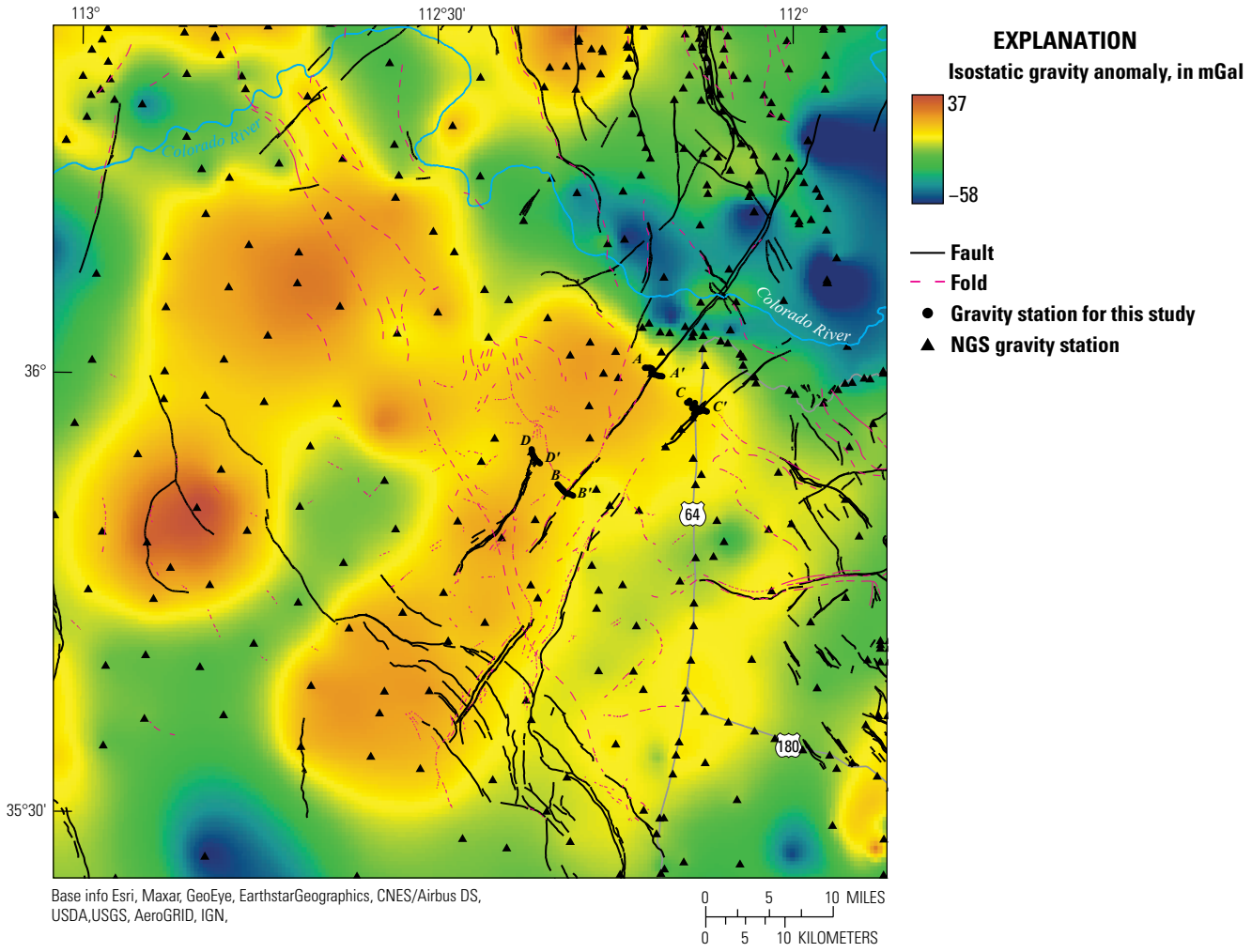

Figure 8. Isostatic gravity anomaly map of the study area in the Coconino Plateau, Coconino County, Arizona, from Sweeney and Hill (2001), with National Geodetic Survey (NGS) gravity observations points (black triangles; Dater and others 1999) and the gravity observation points (black circles) from this study.

that point—a negative gravity anomaly. Three gravity models using the Redlands Ranch Fault Zone were created to compare the magnitude of a negative gravity anomaly resulting from enhanced porosity zones of various widths, where the porosity was scaled by the width (for example, the 1,500 m zone has one third the porosity of the 500 m zone). Values for porosity and width in figure 9*B* were taken from Kessler's model (500 m zones of 0.05 enhanced porosity) (Kessler, 2002) and

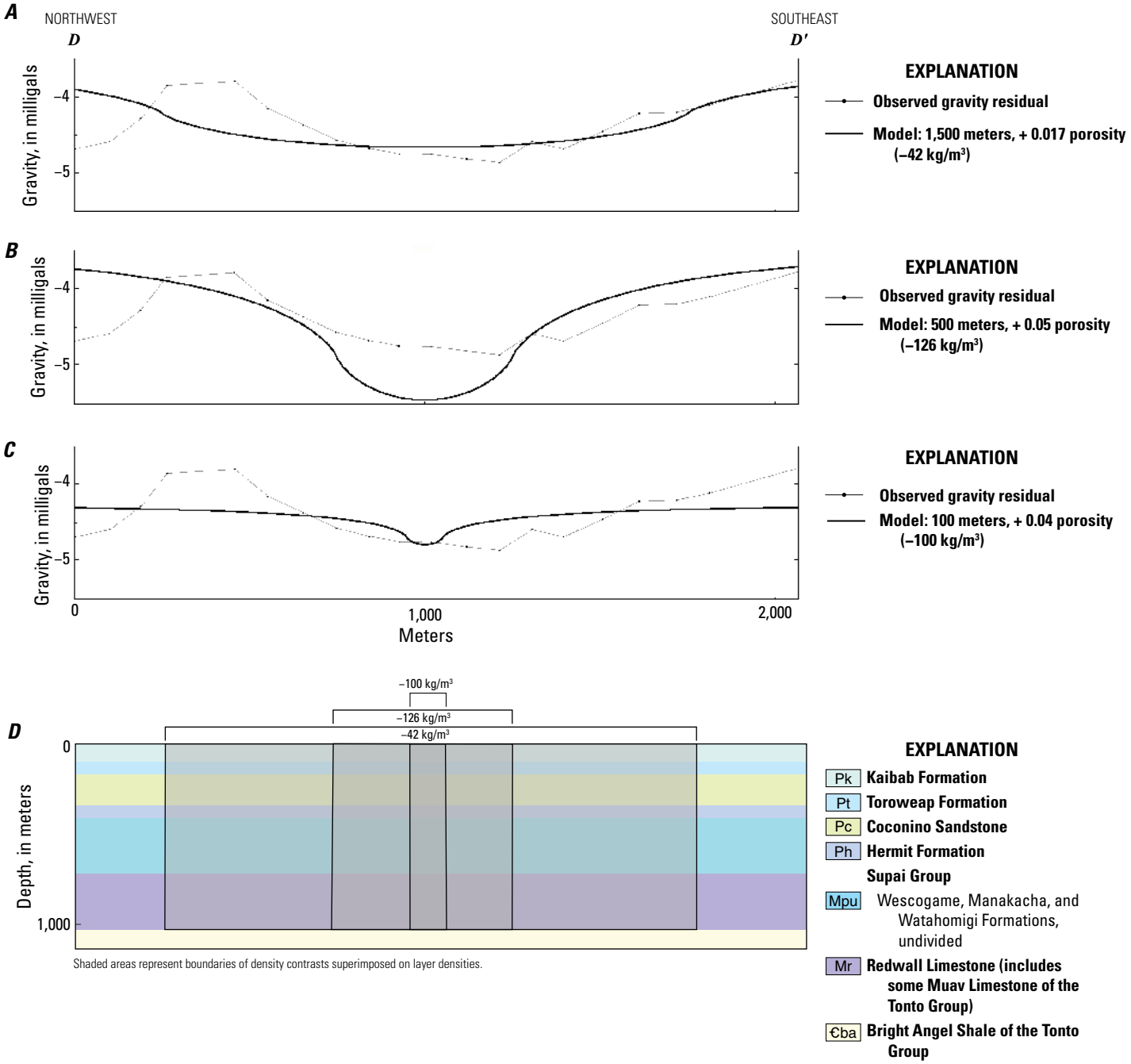

Figure 9. Graphs and diagram showing modeled gravity cross sections and the geology model used to generate modeled gravity residual for the transect of *D* to *D′* across the Redlands Ranch Fault Zone of the Coconino Plateau, north-central Arizona. *A*, Graph showing the 1,500-meter (m)-wide zone of enhanced porosity of 0.017. *B*, Graph showing the 500-m-wide zone of enhanced porosity of 0.05. *C*, Graph showing the 100-m-wide zone of enhanced porosity of 0.04. *D*, Diagram of geology model used to generate the modeled gravity residuals of 9*A*–*C*. Each model (9*A*–*C*) was created using one of the shaded zones of enhanced porosity shown in 9*D*. Enhanced porosity indicates the percentage of additional void space used to determine the density contrast (for example, 0.05 * 2,520 kilograms per cubic meter [kg/m³] = 126 kg/m³; since this is an increase in void space, this corresponds to a decrease in density, so the density contrast is negative: −126 kg/m³).

scaled to a broader zone more representative of earlier work (Montgomery, 1999) in figure 9*A*. The modeled lines in these figures reflect the expected gravity residual resulting from the width and enhanced porosity used in the corresponding groundwater model. The modeled line in figure 9*A* does a better job of staying within the overall magnitude of observed data, but the model in figure 9*B* seems to correspond better with the horizontal bounds of the low in the observed data. The third model (fig. 9*C*) was created to estimate a reasonable minimum anomaly that would be well enough above the level of error to be detected: a 0.5 mGal low across a 100-m-wide 0.04 enhanced porosity zone. Table 2 shows the enhanced porosities, corresponding density contrasts, widths of the enhanced porosity zones, and resulting negative gravity anomalies, in mGal, for each model. Included in table 2 is the modeled gravity anomaly of a 100 m zone of 0.25 enhanced porosity—the proportional porosity used for the models in fig. 9, scaled to 100 m.

Estimated error

Small anomalies present in a gravity residual may be on the order of error if reductions are problematic, and the possibility that apparent anomalies may be the result of other errors should also be considered. Estimated standard deviation of the relative gravity differences measured using the ZLS Burris relative-gravity meter is about 0.003 mGal. Additional error in the vertical accuracy of station elevations obtained using GPS is 0.009 mGal. These errors are small sources of error compared to the accumulated error from gravity reductions, which may be anywhere from 0.1 to 5 mGal (Blakely, 1996). This criterion is for gravity applications requiring only instruments and methods capable of resolution at the mGal level, or as small as 0.01 mGal for studies requiring more careful data collection techniques with instruments considered accurate to the microGal (Deroussi and others, 2009). Many of the gravity reductions rely on observable values for geographical coordinates and elevations that can be measured fairly accurately (e.g. a difference of 1cm in elevation would yield a free air reduction difference of about 0.003 mGal). The error in terrain correction gravity reduction will vary depending on the resolution of the DEM used to model it. Steep terrain modeled as relatively course cubes will produce a less accurate approximation of the terrain than a finer resolution model, or a model of flatter terrain. The Grand Canyon represents the greatest potential source of error in the regional terrain correction, given the proximity of the gravity transects to it and the resolution (100 m) of the elevation grid used for those corrections. Relatively large and rapid changes in elevation along the Bright Angel Fault transect represent the greatest potential for error in the local terrain correction. The effect of a poor local terrain correction will be apparent when comparing the elevation along a transect to the gravity residual.

Table 2. Values used to create modeled gravity responses to zones of enhanced porosity in figure 9.

[Enhanced porosity indicates the percentage of additional void space used to determine the density contrast (e.g., 0.05 * 2,520 kg/m^3 = 126 kg/m^3; since this is an increase in void space, this corresponds to a decrease in density, so the density contrast is negative: –126 kg/m^3.). kg/m^3, kilograms per cubic meter; m, meter; mGal, milligals.]

Enhanced porosity	Density contrast (kg/m^3)	Width (m)	Depth (m)	Anomaly (mGal)
0.05	−126	500	−1,000	−1.7
0.017	−42	1,500	−1,000	−0.8
0.25	−630	100	−1,000	−3.1
0.04	−100	100	−1,000	−0.5

Results

Bright Angel Fault

Two gravity transects separated by about 19 km cross the Bright Angel Fault and Monocline (transects A-A' and B-B', respectively, on fig. 3). For the northernmost gravity transect that crosses the fault (fig. 4), the model incorporates the density contrast between the basement rock on either side of the fault, and the Paleozoic fault offset of 60 m, southeast block down (fig. 10). The elevation of the terrain to either side of the fault is similar, which could suggest that the offset estimated for this fault is too high in this area or could be a result of subsequent erosion or secondary faulting leading to tilting of the west block that also had the effect of lowering the elevation of that block. The modeled gravity presented here assumes 60 m of offset, down to the east, with subsequent erosion resulting in the east block being 60 m thicker than the west. The modeled gravity response based on this geology shows a smooth increase of about 1.3 mGal (northwest to southeast), with no gradient over the fault (fig. 10).

The overall increase in modeled gravity from northwest to southeast is very close to the observed gravity increase in the same direction, which is approximately 1.13 mGal, but the observed gravity residual does not increase smoothly. There is a positive gravity anomaly in the observed residual of approximately 0.5 mGal located over the fault, rather than a negative anomaly as expected if the fault trace represents a zone of enhanced porosity. However, the gravity residual and the elevation appear to be correlated for approximately the first 1,400 m (from northwest to southeast) of the transect (R^2=0.7 for this section, where R^2 is the coefficient of determination). Gravity residuals that are correlated to height may indicate a poor terrain correction or incorrect density used for the terrain correction. Different densities were tested for the terrain correction, but although they resulted in an offset in the gravity residual, they did not change the location or magnitude of the observed anomalies, which suggests the resolution of the terrain correction is poor. Further modeling to account for the anomaly seen in the gravity residual was not done, since these data seem likely to be a result of a non-linear transect and errors with the terrain correction rather than anomalous geology.

There is no indication of a low-density (high-porosity) zone around the fault at this location. If the maximum error for this transect is on the order of a few tenths of a mGal, a –1.7 to –0.8 mGal negative gravity anomaly resulting from a 500 or 1,500 m zone of enhanced porosity (respectively, table 2) should still result in a small negative gravity anomaly, if present.

Bright Angel Monocline

The transect across the Bright Angel Monocline shows a small positive gravity anomaly of approximately 0.5 mGal roughly corresponding to exposed Kaibab Formation (fig. 5). The geologic model simulated a short segment of uplift to the northwest similar to the expected geology of an anticline, which

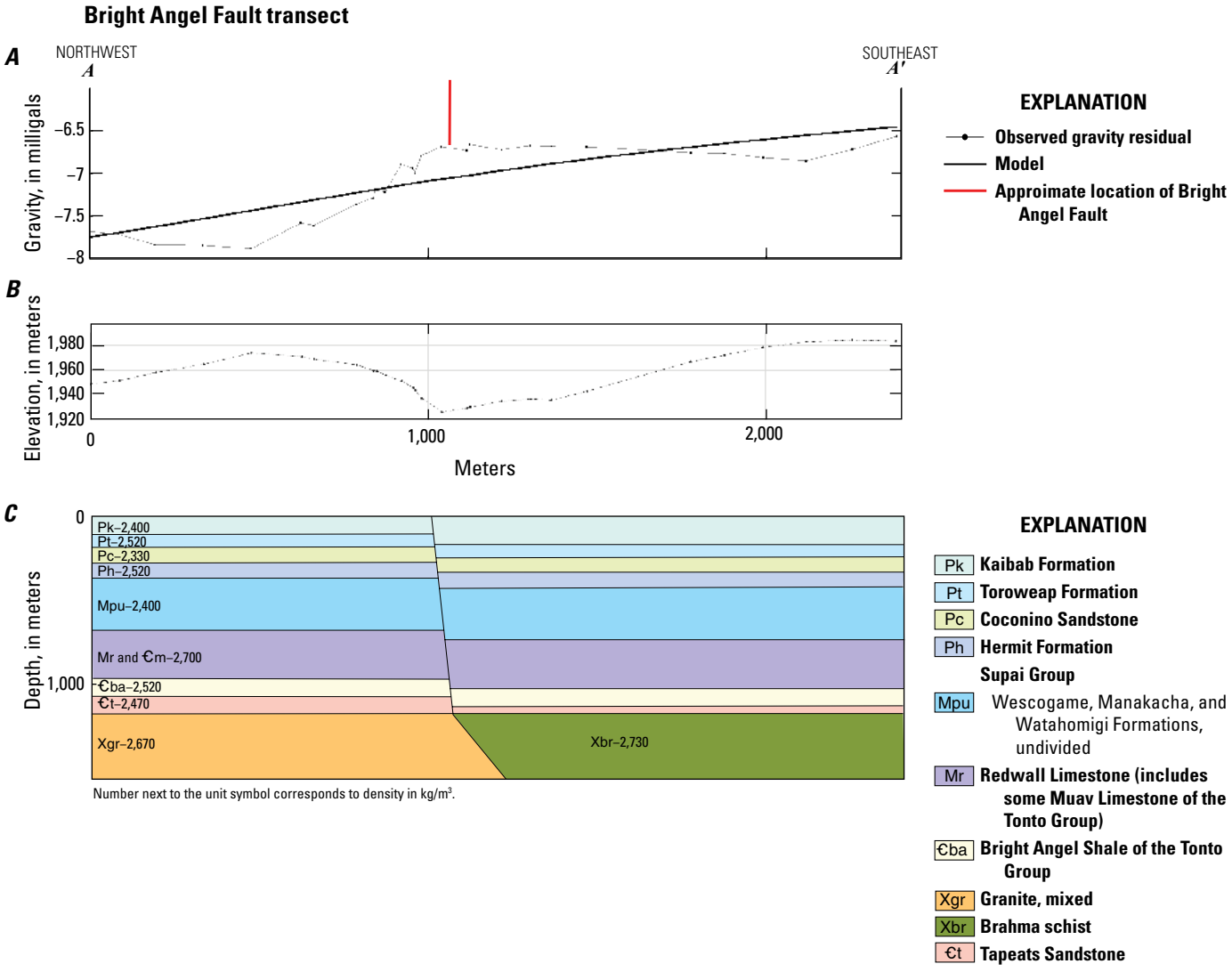

Figure 10. Gravity residual model (*A* to *A′*) across the Bright Angel Fault (fig. 4), in the Coconino Plateau, Coconino County, Arizona. *A*, the observed and modeled gravity residuals; *B*, elevation at corresponding gravity observation points in figure 10*A*; and *C*, geology model used to generate modeled gravity residual in figure 10*A*. The red line in *A* shows the approximate location of the Bright Angel Fault. The model incorporates the density contrast between the basement rock on either side of the fault, and the Paleozoic fault offset of 60 meters, southeast block down. The modeled gravity response based on this geology shows a smooth increase of about 1.3 milligals (northwest to southeast), with no gradient over the fault. There is no indication of a low-density/high-porosity zone around the fault at this location. kg/m³, kilograms per cubic meter.

resulted in modeled gravity with good fit to the observed gravity residual (fig. 11). The modeled lift of the fold was 60 m, similar to the offset documented in the Bright Angel Fault. The R^2 value of 0.31 for this transect indicates relatively low correlation between station elevation and observed gravity residual. A high R^2 value would indicate that the observed gravity residual could be well-modeled as a function of elevation, rather than anomalous geology, and would suggest a poor reduction. The gravity residual for this transect does not appear to be affected by the potential density contrast of basement rock on either side of the monocline axis. It cannot be confirmed if there is such a density contrast across the axis of the monocline in this location. The data for this transect do appear to show a justifiable anomaly related to the monocline, but there are no negative gravity anomalies along the transect that would indicate a low-density zone associated with the feature.

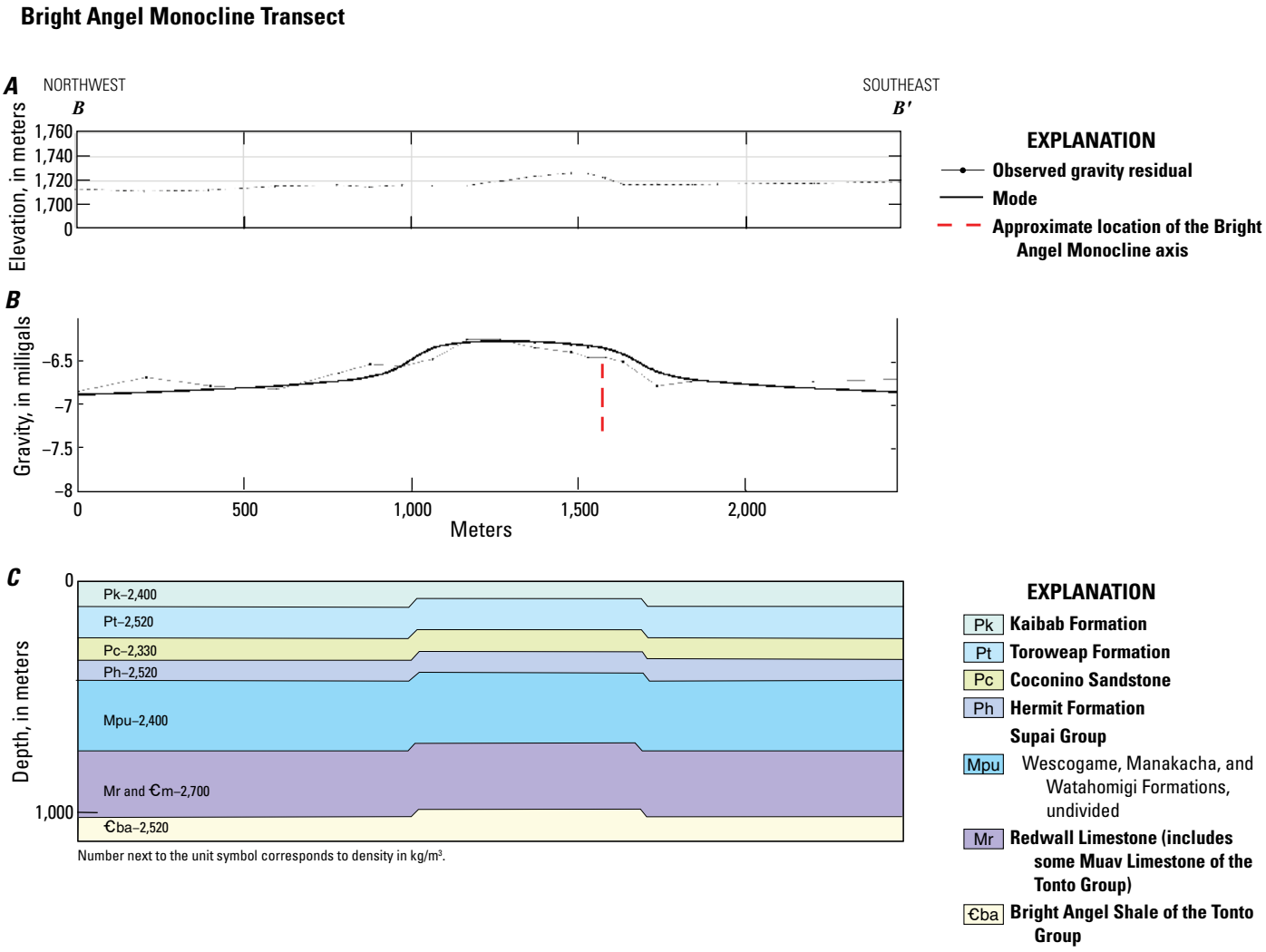

Figure 11. Gravity residual model (*B* to *B′*) of the Bright Angel Monocline (fig. 5), in the Coconino Plateau, Coconino County, Arizona. *A*, the observed and modeled gravity residuals; *B*, elevation at corresponding gravity observation points in figure 11*A*; and *C*, geology model used to generate modeled gravity residual in figure 11*A*.The dashed red line shows the approximate location of the monocline axis. The geologic model simulated a short segment of uplift to the northwest similar to the expected geology of an anticline, which resulted in modeled gravity with good fit to the observed gravity residual. The gravity residual for this transect does not appear to be affected by the potential density contrast of basement rock on either side of the monocline axis. The data for this transect do appear to show a justifiable anomaly related to the monocline, but there are no negative gravity anomalies along the transect that would indicate a low-density zone associated with the feature. kg/m³, kilograms per cubic meter.

Tusayan Graben

The gravity residual for the Tusayan Graben shows a very small, steep gradient down near the western bounding fault, followed by a positive gravity anomaly of approximately 0.6 mGal at about the location of the fault bounding the east side of the graben (fig. 12). The geologic model used for the modeled gravity residual is based on the dimensions of the graben in the transect, and an asymmetrical downdrop of about 10 m, which is based on the topography of the graben. This model produces a negative gravity anomaly, resulting from Kaibab Formation to either side of the graben juxtaposed with less dense alluvium within the graben (fig. 6). A negative density contrast produces a negative gravity anomaly, inconsistent with the observed positive anomaly. The positive observed anomaly suggests that the geologic model is missing information, such as possible involvement of the bedrock that is unknown. Errors in the data are likely at least partially responsible for the anomaly. There are two sections of the transect where observed gravity residual and gravity station elevation are apparently related, with R^2 greater than or equal to 0.5 for both sections. For approximately the first 1,800 m from northwest to southeast along the transect, the gravity residual is increasing with increasing elevation, but continuing between 1,900 and 2,600 m the gravity residual is decreasing with increasing elevation. These data were also collected along a transect that was not a straight line but were projected onto a line formed between the first and last data points of the transect, which may introduce additional error. Additional modeling was considered unjustified since the accumulated error is likely on the same order as the observed anomaly.

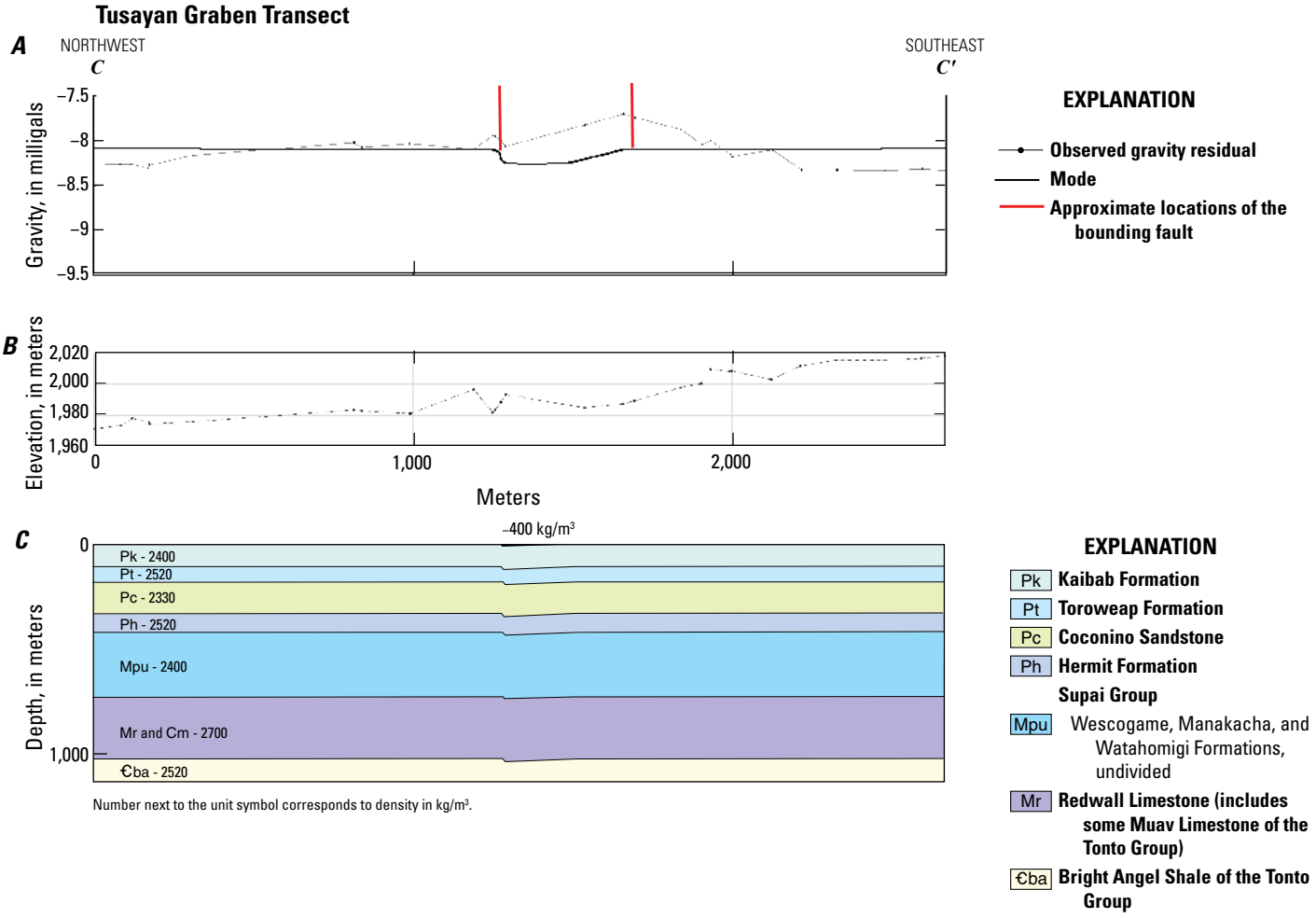

Figure 12. Gravity residual model (*C* to *C*′) for Tusayan Graben (fig. 6), in the Coconino Plateau, Coconino County, Arizona. *A*, the observed and modeled gravity residuals; *B*, elevation at corresponding gravity observation points in figure 12*A*; and *C*, geology model used to generate modeled gravity residual in figure 12*A*. The geologic model used for the modeled gravity residual is based on the dimensions of the graben in the transect, and an asymmetrical downdrop of about 10 meters, which is based on the topography of the graben. This model produces a negative gravity anomaly, resulting from Kaibab Formation to either side of the graben juxtaposed with less dense alluvium within the Graben (fig. 6). A negative density contrast produces a negative gravity anomaly, inconsistent with the observed positive anomaly. Red lines indicate the approximate locations of the bounding faults of the graben. kg/m³, kilograms per cubic meter.

Redlands Ranch Fault Zone

The gravity residual for this transect shows a negative gravity anomaly that smoothly transitions to a positive anomaly on either side (fig. 13). The negative anomaly was roughly matched by modeling a zone 800 m wide and 1,000 m deep, with a porosity increase of 0.017 (0.017 multiplied by the average Paleozoic strata density of 2,520 kg/m^3 results in a density change of –42 kg/m^3). One fault line crosses the transect, and two other faults approach it, as do three collapse features (fig. 5). The enhanced porosity zone modeled in figure 13 was placed so that the modeled gravity was as close as possible to the observed gravity residual. This placement puts the zone of enhanced porosity almost directly between the two outermost faults, suggesting they bound the lower density zone. However, the enhanced porosity zone of 800 m only accounted for a negative anomaly of 0.75 mGal in the modeled gravity and did not account for the positive gravity anomalies to either side of the feature, or the relatively large negative anomaly to the northwest. These were not modeled owing to lack of geologic information in this area.

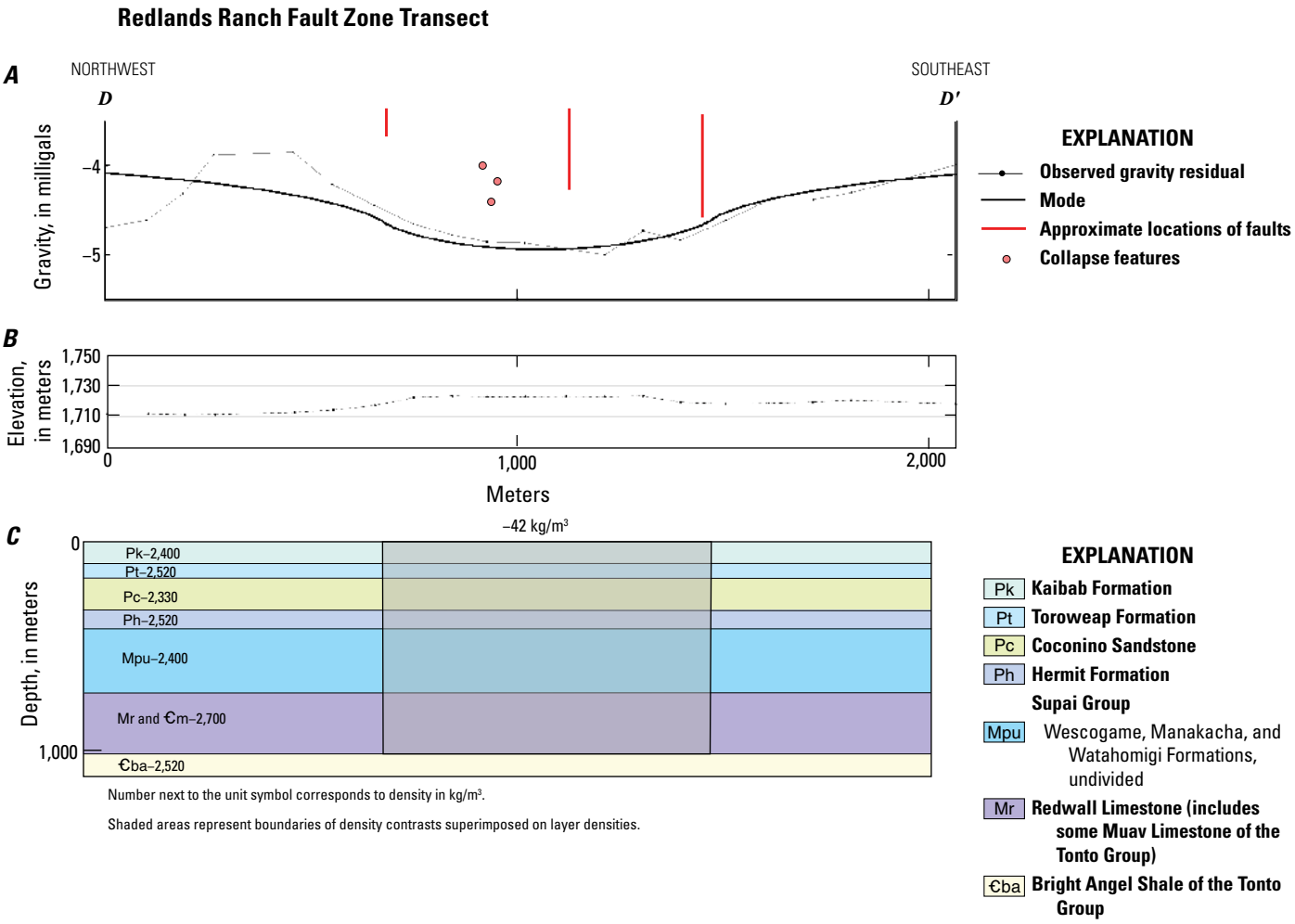

Figure 13. Gravity residual model (*D* to *D′*) for Redlands Ranch Fault Zone transect, in the Coconino Plateau, Coconino County, Arizona. *A*, the observed and modeled gravity residuals; *B*, elevation at corresponding gravity observation points in figure 13*A*; and *C*, geology model used to generate modeled gravity residual in figure 13*A*. Red lines indicate the approximate locations of nearby faults, and red circles the approximate locations of collapse features; distance from the gravity residual line corresponds to relative distance of each feature from the gravity observation points for this transect. The gravity residual shows a negative gravity anomaly that smoothly transitions to a positive anomaly on either side. The negative anomaly was roughly matched by modeling a zone 800 meters (m) wide and 1,000 m deep, with a porosity increase of 0. The enhanced porosity zone was placed so that the modeled gravity was as close as possible to the observed gravity residual. kg/m^3, kilograms per cubic meter.

Gravity Transect Comparisons

The observed gravity residuals for the four gravity transects from this study were compared to the isostatic residual anomalies from Sweeny and Hill (2001) at the same locations as the gravity station elevation (fig. 14).

Three of the gravity transects, the Bright Angel Fault, Bright Angel Monocline, and Tusayan Graben, showed no indication of zones of enhanced porosity within 1 km on either side of the faults or fold. Two of the gravity transects (Bright Angel Fault and Tusayan Graben), showed small positive gravity anomalies which were similar in shape and size to the anomalies in the Sweeney and Hill (2001) gravity residuals (extracted to the same points as observations for this study (fig. 14*A*). NGS stations along or near the Tusayan Graben also indicate greater gravity in the part of the graben where the transect for this study was completed, and lower gravity near the bottom third of the graben (Dater and others, 1999; fig. 6). Taken together, it seems likely that there is a valid geologic reason why the gravity residual shows a positive anomaly over the graben rather than a negative one. However, the similarity between the gravity residual for the Bright Angel Fault and the isostatic gravity residual of Sweeney and Hill (2001) likely results from the shape of the transect. The section of the transect to the northwest of the fault is slightly offset to the north relative to the southeast section (fig. 4). FastGrav (Price, 2020) projects all transect points onto a line extending between the endpoints of the transect, but it is possible that the difference in the gravity residual on either side of the fault may be due to a trend that influences observation points as a function of distance along the fault, rather than a genuine geologic anomaly. The isostatic gravity anomaly map of Sweeney and Hill (2001) also shows decreasing gravity along the fault in this area, towards the Grand Canyon, which further suggests this is not an anomaly but an artefact of a regional trend (fig. 8).

Discussion and Conclusions

The one observed negative gravity anomaly, in the Redlands Ranch Fault Zone transect, shows a low-density zone lying between the two outermost faults that approach or cross the transect (fig. 13). The presence of the collapse features approaching the transect may be an indication that collapse features could play a larger role in locating enhanced porosity zones, but additional work would need to be done to test this. A shallower zone of higher porosity (affecting only the strata of the Kaibab and Toroweap Formations) could produce a negative gravity anomaly of similar size with somewhat steeper gradients on either side, but a deeper zone of enhanced porosity (exclusively in the R aquifer, for example) would result in shallower and more extensive gradients on either side of the negative gravity anomaly that would not resemble the observed gravity residual. Therefore, the negative gravity anomaly observed near the middle of this transect is likely a result of a relatively shallow negative density contrast, as modeled (fig. 13). An extension of this transect further to the northwest could be useful in identifying the source of the negative anomaly on the northwest edge of the transect, and additional work could be carried out to attempt to identify the source of the positive gravity anomaly bounding the negative anomaly on the northwest.

The small positive anomaly over the Bright Angel Monocline is more typical of an anticline, which suggests the extent of the uplifted northwest limb of the monocline may be quite limited in the area of the transect, more typical of an anticline. The terrain is largely smooth and flat, which likely introduced little error in the gravity residual (fig. 9). The anomalies in the gravity residuals at the locations from figure 3 are likely valid, resulting from geologic features of anomalous density, though the exact dimensions and density contrasts cannot be determined. The isostatic gravity residuals from Sweeney and Hill, (2001) for Bright Angel Fault and Redlands Ranch Fault Zone gravity transects in this area are almost completely linear but the resolution of the data collected here is higher (fig. 13*A*).

The results of this study indicate that additional work on collapse features may prove useful for identifying other negative gravity anomalies that could indicate high porosity zones. The work of Gettings and Bultman (2005) could also be considered when identifying features of interest for further study, including those that may represent deep penetrative fractures where water from the C aquifer or the surface may recharge the R aquifer or where low-density fault cores may create sections of conduit flow along the fault. Finally, additional data collection to aid in mapping the location and extents of the upper aquifer system on the Coconino Plateau may represent a useful means to improve model calculations, as estimated connectivity between the aquifers implied by Solder and others (2020) may also help improve model results.

This study identified one negative gravity anomaly across the Redlands Ranch Fault Zone that was modeled within the width and enhanced porosity values of those used in groundwater models of the area. This study was unable to verify the existence of enhanced porosity zones at the chosen locations along two major northeast-southwest features, the Bright Angel Fault and Tusayan Graben, which have been modeled as continuous zones of enhanced porosity. However, faults and other features may affect groundwater flow in different ways at different locations, and this work does not preclude the existence of enhanced porosity zones at other places along these features. Identifying locations where geologic features have resulted in enhanced porosity zones that could be preferential flow paths could be useful for understanding effects of future pumping on springs and groundwater availability on the Coconino Plateau. The magnitude of all the gravity residual anomalies presented here are relatively small magnitude (<1 mGal) and may also have relatively large error associated with them (estimated here to be one to several tenths of a mGal). Additional gravity data collection could be useful in testing the results presented here and attempting to identify other zones of enhanced

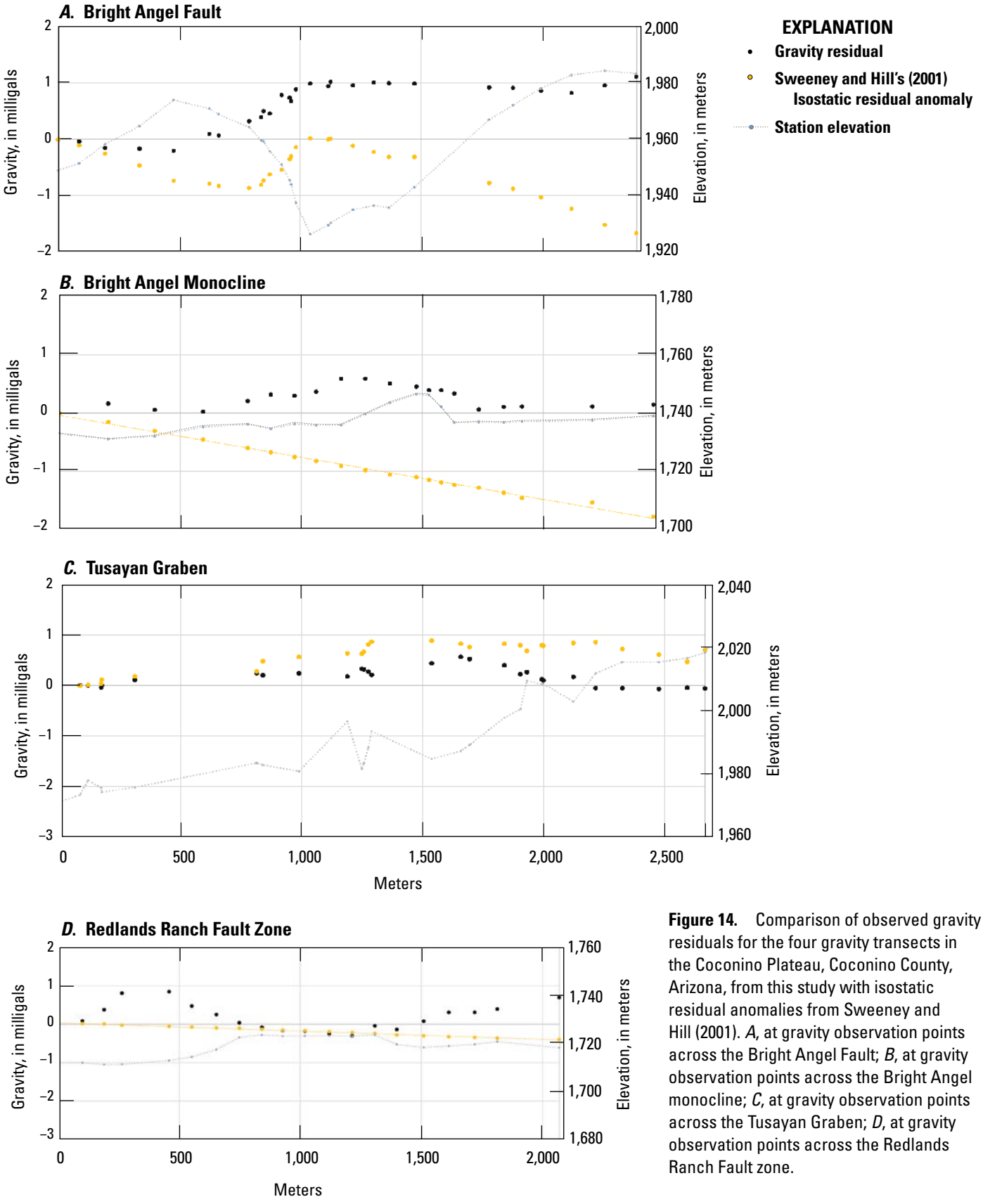

Figure 14. Comparison of observed gravity residuals for the four gravity transects in the Coconino Plateau, Coconino County, Arizona, from this study with isostatic residual anomalies from Sweeney and Hill (2001). *A*, at gravity observation points across the Bright Angel Fault; *B*, at gravity observation points across the Bright Angel monocline; *C*, at gravity observation points across the Tusayan Graben; *D*, at gravity observation points across the Redlands Ranch Fault zone.

porosity near or along features. However, the depth of zones of enhanced porosity is also a limiting factor to this type of work; it is possible that such zones are limited to the karstic R aquifer, which would make them too deep to detect with practical surface geophysics. If this were determined to be the case, groundwater models of the area could be improved by additional observation data, rather than additional work such as was carried out in this study.

Data Availability

This report is accompanied by a USGS data release (Wildermuth, 2021) that contains gravity observation data (relative gravity data) adjusted by combining gravity observations from this study with absolute gravity values from nearby NGS gravity observation locations (Dater and others, 1999) using GSadjust (Kennedy, 2020). Values for the corrections listed in equation 1 are also given, as calculated using QCTool (Petros Eikon, Inc., 2018), along with the resulting gravity residual values reported here. These data may be used to duplicate the results shown in this report and provide additional information about the correction values at each gravity observation point.

Acknowledgements

This investigation was supported by the USGS Toxic Substances Hydrology Program.-

References Cited

Arizona Department of Water Resources (ADWR), 2020, ADWR tabular data download, Groundwater Site Inventory (GWSI) and Wells 55 Registry: Arizona Department of Water Resources, accessed 10/2020, at https://new.azwater.gov/gis.

Beus, S.S., and Morales, M., eds., 1990, Grand Canyon geology: New York and Flagstaff, Oxford University Press and Museum of Northern Arizona Press, 518 p.

Billingsley, G.H., 2000, Geologic map of the Grand Canyon 30’ × 60’ quadrangle, Coconino and Mohave Counties, northwestern Arizona: U.S. Geological Survey Geologic Investigations Map I–2688, 15 p., scale 1:100,000, https://doi.org/10.3133/i2688.

Billingsley, G.H., Felger, T.L., and Priest, S.S., 2006, Geologic map of the Valle 30’ × 60’ quadrangle, Coconino County, northern Arizona: U.S. Geological Survey Geologic Investigations Map 2895, 27 p., scale 1:100,000, https://doi.org/10.3133/sim2895.

Billingsley, G.H., and Hendricks, J.D., 1989, Physiographic features of northwestern Arizona, chap 4 *of* Elston, D.P., Billingsley, G.H., and Young, R.A., eds., Geology of Grand Canyon, northern Arizona (with Colorado River guides)—Lee Ferry to Pierce Ferry, Arizona, v. 115: Washington, D.C., American Geophysical Union, Field Trip Guidebook Series, p. 67–71.

Bills., D.J., Truini, Margot, Flynn, M.E., Pierce, H.E., Catchings, R.D., and Rymer, M.J., 2000, Hydrogeology of the regional aquifer near Flagstaff, Arizona: U.S. Geological Survey Water-Resources Investigations Report 00-4122, 143 p., 4 plates, https://doi.org/10.3133/wri004122.

Bills, D.J., and Flynn M.E., 2002, Hydrogeologic data for the Coconino Plateau and adjacent areas, Coconino and Yavapai Counties, Arizona: U.S. Geological Survey Open-File Report 2002–265, 29 p., https://doi.org/10.3133/ofr02265.

Bills, D.J., Flynn, M.E., and Monroe, S.A., 2016, Hydrogeology of the Coconino Plateau and adjacent areas, Coconino and Yavapai Counties, Arizona (ver. 1.1): U.S. Geological Survey Scientific Investigations Report 2005–5222, 101 p., 4 pl., https://doi.org/10.3133/sir20055222.

Blakely, R.J., 1996, Potential theory in gravity and magnetic applications: Cambridge University Press, 441 p.

Darton, N.H., 1910, A reconnaissance of parts of northwestern New Mexico and northern Arizona: U.S. Geological Survey Bulletin 435, 88 p., 1 pl., https://doi.org/10.3133/b435.

Dater D., Metzger, D., and Hittelman, A., comps., Land and marine gravity CD-ROMs, 1999: U.S. Department of Commerce, National Oceanic and Atmospheric Administration, National Geophysical Data Center, Boulder, Colo., 2 CD-ROMs.

Deroussi, S., Diament, M., Feret, J.B., Nebut, T., and Staudacher, T., 2009, Localization of cavities in a thick lava flow by microgravimetry: Journal of Volcanology and Geothermal Research, v. 184, issues 1–2, p. 193–198, https://doi.org/10.1016/j.jvolgeores.2008.10.002.

Dutton, C.E., 1882, Atlas to accompany the monograph on the Tertiary history of the Grand Cañon district: U.S. Geological Survey Monograph 2, 264 p., 23 sheets, scale 1:250,000, https://doi.org/10.3133/m2_1882.

Dutson, S.J., 2005, Effects of Hurricane fault architecture on groundwater flow in the Timpoweap Canyon of southwestern Utah: Provo, Utah, Brigham Young University, M.S. thesis, 66 p., accessed 10/18/2021, at https://scholarsarchive.byu.edu/etd/583/.

Esri Inc., 2020. *ArcGIS Pro* (Version 2.5.2). Esri Inc. https://www.esri.com/en-us/arcgis/products/arcgis-pro/overview.

Gettings, M.E., and Bultman, M.W., 2005, Candidate-penetrative-fracture mapping of the Grand Canyon area, Arizona, from spatial correlation of deep geophysical features and surficial lineaments: U.S. Geological Survey Data Series 121, https://doi.org/10.3133/ds121. [Also available as 1 DVD.]

Hart, R.J., Ward, J.J., Bills, D.J., and Flynn, M.E., 2002, Generalized hydrogeology and ground-water budget for the C Aquifer, Little Colorado River Basin and parts of the Verde and Salt River Basins, Arizona and New Mexico: U.S. Geological Survey Water-Resources Investigations Report 2002–4026, 47 p., https://doi.org/10.3133/wri024026.

Hunt, C.B., 1967, Physiography of the United States: San Francisco, W.H. Freeman and Co. Ltd., 630 p.

Huntoon, P.W., 1974, Synopsis of Laramide and post Laramide structural geology of the eastern Grand Canyon, Arizona, *in* Karlstrom, T.N.V., Swann, G.A., and Eastwood, R.L., eds., Geology of northern Arizona with notes on archaeology and paleoclimate, Part 1, Regional studies: Geological Society of America, Rocky Mountain Section Meeting, Flagstaff, Arizona, p. 317–335.

Huntoon, P.W., 1977, Relationship of tectonic structure to aquifer mechanics in the western Grand Canyon district Arizona: Laramie, University of Wyoming, Water Resources Research Institute, Water Resources Series no. 66, 51 p., 2 pls., accessed 10/2020, http://library.wrds.uwyo.edu/wrs/wrs-66/wrs-66-co.html.

Huntoon, P.W., Sears, J.W., 1975, Bright Angel and Eminence faults, eastern Grand Canyon, Arizona: Geological Society of American Bulletin, v. 86, no. 4, p. 465–472, https://doi.org/10.1130/0016-7606(1975)86<465:BAAEFE>2.0.CO;2.

Hurlow, H.A., 1998, The geology of the central Virgin River basin, southwestern Utah, and its relation to ground-water conditions: Utah Geological Survey Water-Resources Bulletin no. 26, 65 p., accessed 10/2020 at https://ugspub.nr.utah.gov/publications/water_resources_bulletins/wrb-26.pdf.

Hwang, C., Wang, C., and Lee, L., 2002, Adjustment of relative gravity measurements using weighted and datum-free constraints: Computers and Geoscience, v. 28, issue 9, p. 1005–1015., https://doi.org/10.1016/S0098-3004(02)00005-5.

Ilg, B.R., Karlstrom, K. E., Hawkins, D.P., Williams, M.L., 1996, Tectonic evolution of Paleoproterozoic rocks in the Grand Canyon—Insights into middle-crustal processes: GSA Bulletin, v. 108, n. 9, p. 1149–1166, https://doi.org/10.1130/0016-7606(1996)108<1149:TEOPRI>2.3.CO;2.

Inkenbrandt, P., Thomas, K., and Jordan, J.L., 2013, Regional groundwater flow and water quality in the Virgin River basin and surrounding areas, Utah and Arizona: Utah Geological Survey Report of Investigation 272., accessed 10/2020 at https://geology.utah.gov/regional-groundwater-flow-and-water-quality-in-the-virgin-river-basin-and-surrounding-areas-utah-and-surrounding-areas-utah-and-arizona/.

Kennedy, J., 2020, GSadjust v1.0: U.S. Geological Survey Software Release, 20 December 2020, https://doi.org/10.5066/P9YEIOU8.

Kessler, J.A., 2002, Grand Canyon springs and the Redwall Muav aquifer—Comparison of geologic framework and groundwater flow models: Flagstaff, Ariz., Northern Arizona University, M.S. thesis, 122 p.

Lockrem, T.M., and Best, D.M, 1983, Gravity modeling of the Slate Mountain volcano-laccolith, Coconino County, Arizona: Journal of the Arizona-Nevada Academy of Science, v. 18, no. 2, p. 69-74, accessed 11/2020 at https://www.jstor.org/stable/27641691.

McCallum, J., Simmons, C., Mallants, D., and Batelaan, O., 2018, Simulating the groundwater flow dynamics of fault zones: Adelaide, South Australia, Flinders University, National Centre for Groundwater Research and Training, 52 p., accessed 10/2020 at https://www.environment.gov.au/system/files/resources/877d5b40-4269-4708-a55f-b5e25df21b4b/files/simulating-the-groundwater-flow-dynamics-of-fault-zones.pdf.

Metzger, D.G., 1961, Geology in relation to availability of water along the south rim, Grand Canyon National Park, Arizona: U.S. Geological Survey Water-Supply Paper 1475–C, 138 p., 2 pl., https://doi.org/10.3133/wsp1475C.

Montgomery, E.L., 1999, Supplemental assessment of hydrogeologic conditions and potential effects of proposed groundwater withdrawal Coconino Plateau Groundwater Sub-basin, Coconino County [appendix], Record of Decision, Final Environmental Impact Statement for Tusayan Growth—Kaibab National Forest, Williams, Ariz., July 1999: U.S. Department of Agriculture, Forest Service, Southwestern Region, 256 p.

Petros Eikon, Inc., 2018, QCTool software version 3.10: Orangeville, Ontario, Canada, Petros Eikon, Inc., accessed 10/2020, at https://www.qc-tool.com/.

Phelps, G., Cronkite-Ratcliff, C., and Klofas, L., 2013, Principal facts and an approach to collecting gravity data using near real-time observations in the vicinity of Barstow, California: U.S. Geological Survey Open-File Report 2013–1264, 24 p., http://pubs.usgs.gov/of/2013/1264/.

Pool, D.R., Blasch, K.W., Callegary, J.B., Leake, S.A., and Graser, L.F., 2011, Regional groundwater-flow model of the Redwall-Muav, Coconino, and alluvial basin aquifer systems of northern and central Arizona: U.S. Geological Survey Scientific Investigations Report 2010–5180, v. 1.1, 118 p., https://doi.org/10.3133/sir20105180.

Price, A.M., 2020, FastGrav, ver. 0.9.0: Aaron Price, accessed 10/2020 at http://fastgrav.com/.

Prieto, C., 1996, Gravity/magnetic signatures of various geologic models—An exercise in pattern recognition: Houston, Tex., Integrated Geophysics Corporation Footnote Series, v. 4, no. 4, https://doi.org/10.1190/1.9781560801832.

Savage, H.M., and Brodsky, E.E., 2011, Collateral damage—Evolution with displacement of fracture distribution and secondary fault strands in fault damage zones: Journal of Geophysical Research, v. 116, B03405, 14 p, https://doi.org/10.1029/2010JB007665.

Shoemaker, E.M., Squires, R.L., and Abrams, M.J., 1978, Bright Angel and Mesa Butte Fault systems of northern Arizona, *in* Smith, R.B., and Eaton, G.P., eds., Cenozoic tectonics and regional geophysics of the western Cordillera: Geological Society of America Memoir 152, p. 341–367.

Solder, J.E., Beisner, K.R., Anderson, J., and Bills, D.J., 2020, Rethinking groundwater flow on the South Rim of the Grand Canyon, USA—Characterizing recharge sources and flow paths with environmental tracers: Hydrogeology Journal v. 28, no. 1593–1613, https://doi.org/10.1007/s10040-020-02193-z.

Spamer, E.E., comp., 1990, Bibliography of the Grand Canyon and the Lower Colorado River from 1540: Grand Canyon Natural History Association, Grand Canyon, Arizona, Monograph 8, 360 p.

Sweeney, R.E., and Hill, P.L., 2001, Arizona aeromagnetic and gravity maps and data—A web site for distribution of data: U.S. Geological Survey Open-File Report 2001–81, ver. 1.0, accessed July 30, 2020, at https://doi.org/10.3133/ofr0181.

Talwani, M., and Ewing, M., 1960, Rapid computation of gravitational attraction of three-dimensional bodies of arbitrary shape: Geophysics v. 25, issue 1, p. 203–225, https://doi.org/10.1190/1.1438687.

U.S. Geological Survey, 2020, 3D Elevation Program (3DEP): U.S. Geological Survey, The National Map 3D Elevation Program, accessed July 30, 2020, at https://www.usgs.gov/core-science-systems/ngp/3dep.

Weir, G.W., Ulrich, G.E., and Nealey, D.L., 1989, Geologic map of the Sedona 30’ × 60’ quadrangle, Yavapai and Coconino Counties, Arizona: U.S. Geological Survey Miscellaneous Investigations Series Map I–1896, 1 sheet, scale, 1:100,000, https://doi.org/10.3133/i1896.

Wildermuth, L.M., 2021, Data from “Gravity surveys for estimating possible width of enhanced porosity zones across structures on the Coconino Plateau, Coconino County, north-central Arizona: U.S. Geological Survey data release, https://doi.org/10.5066/P9ZYHEBB.

Moffett Field Publishing Service Center, California
Manuscript approved for publication March 14, 2022
Edited by Mitchell Phillips
Illustrative support by Katie Sullivan
Layout by Kimber Petersen

ISSN 2328-0328 (online)
https://doi.org/10.3133/sir20225031